



UNIVERSITY OF LEEDS

This is a repository copy of *Effects of heat treatment on the atomic structure and surface energy of rutile and anatase TiO<sub>2</sub> nanoparticles under vacuum and water environments*.

White Rose Research Online URL for this paper:  
<http://eprints.whiterose.ac.uk/95585/>

Version: Accepted Version

---

**Article:**

Okeke, G, Hammond, RB and Antony, SJ (2016) Effects of heat treatment on the atomic structure and surface energy of rutile and anatase TiO<sub>2</sub> nanoparticles under vacuum and water environments. *Chemical Engineering Science*, 146. pp. 144-158. ISSN 0009-2509

<https://doi.org/10.1016/j.ces.2016.02.035>

---

© 2016, Elsevier. Licensed under the Creative Commons Attribution-NonCommercial-NoDerivatives 4.0 International  
<http://creativecommons.org/licenses/by-nc-nd/4.0/>

**Reuse**

Unless indicated otherwise, fulltext items are protected by copyright with all rights reserved. The copyright exception in section 29 of the Copyright, Designs and Patents Act 1988 allows the making of a single copy solely for the purpose of non-commercial research or private study within the limits of fair dealing. The publisher or other rights-holder may allow further reproduction and re-use of this version - refer to the White Rose Research Online record for this item. Where records identify the publisher as the copyright holder, users can verify any specific terms of use on the publisher's website.

**Takedown**

If you consider content in White Rose Research Online to be in breach of UK law, please notify us by emailing [eprints@whiterose.ac.uk](mailto:eprints@whiterose.ac.uk) including the URL of the record and the reason for the withdrawal request.



[eprints@whiterose.ac.uk](mailto:eprints@whiterose.ac.uk)  
<https://eprints.whiterose.ac.uk/>

2

3 **Effects of heat treatment on the atomic structure and surface**  
4 **energy of rutile and anatase TiO<sub>2</sub> nanoparticles under vacuum**  
5 **and water environments**

6 George Okeke, Robert B. Hammond, S. Joseph Antony\*

7 School of Chemical and Process Engineering, University of Leeds, Leeds LS2 9JT, UK

8 \*Corresponding author: [S.J.Antony@leeds.ac.uk](mailto:S.J.Antony@leeds.ac.uk)

9

10 **Abstract**

11 Nanomaterials have become a widely used group of materials in many chemical engineering  
12 applications owing to their ability to provide an enhanced level of functional properties  
13 compared to their crystalline and bulk counterparts. Here we report fundamental level  
14 advancements on how the anatase and rutile phase of TiO<sub>2</sub> nanoparticles chemo-thermally  
15 respond between room temperature and the melting temperature under both vacuum and water  
16 environments. The current study is based on using molecular dynamics (MD) simulations. We  
17 present results on the equilibrium crystal morphology of these phases, structural and surface  
18 energy of TiO<sub>2</sub> nanoparticles in the size range of 2-6 nm under different temperatures.  
19 Thermodynamic and structural properties, in the form of potential energy and Radial  
20 Distribution Functions (RDF's) respectively, are calculated for both forms of TiO<sub>2</sub>  
21 nanoparticles. The temperature associated with the melting transition increased with an  
22 increase in the particle size in both the phases. The potential energy change associated with  
23 the melting transition for anatase was seen to be less than that for rutile nanoparticles. Also  
24 the temperature at which the RDF's began to stretch and broaden was observed to be lower for

25 the case of anatase than rutile, suggesting that rutile attains the most thermal stable phase for  
26 the nano particle sizes considered in this study. Structural changes in anatase and rutile  
27 nanoparticles under different temperatures revealed that non-spherical (rod-like) rutile  
28 nanoparticles tend to be thermodynamically more stable. Surface energy influences the shape  
29 of TiO<sub>2</sub> nanoparticles at different temperatures. The increase in the surface energy of  
30 nanoparticles under vacuum when compared with that of water environment is higher for the  
31 anatase phase than the rutile phase of nanoparticle sizes studied here. The fundamental level  
32 simulation results reported here provide a strong platform for potentially accounting for the  
33 effects of atomic-scale phase characteristics of TiO<sub>2</sub> nanoparticles and surface energy under  
34 different temperature fields in nano processing applications and related multi-scale modelling  
35 approaches in future.

36 **Keywords:** MD simulations, RDF, surface energy, potential energy, anatase, rutile, titania

## 37 **1 Introduction**

38 There is growing interest in understanding the material properties of nano-particles, and their  
39 link to the performance of nano-particulate dispersions, via modelling over multiple length and  
40 time scales. Nano-particles are employed in a number of important engineering applications  
41 for example nanofluids for enhanced thermal conductivity. Nanofluids containing titanium  
42 dioxide (TiO<sub>2</sub>) nanoparticles have been investigated in terms of the particle-scale properties  
43 (Okeke et al., 2011; Okeke et al., 2013a). Metal oxide and ceramic particles at the nanometer  
44 size can be used in a variety of application areas such as chemical sensors (Zheng et al., 2000),  
45 electronics, microporous membranes (Kermanpur et al., 2008), photocatalysis (Onozuka et al.,  
46 2006) and catalysis (Soo-Jin Park, 2010; Hu et al., 2002; Xia et al., 2003; Chaudhari et al.,  
47 2006; Chen and Weng, 2005; Haverkamp, 2010; Park et al., 2010). Ceramic particles at  
48 nanometer sizes have a large surface area per unit mass which may, potentially, enhance

49 physical, chemical and electrical properties compared to the corresponding properties in the  
50 bulk state.

51 The uses of titania in nanotechnology have been investigated widely as it possesses many  
52 desirable properties such as low cost, recyclability, and ease of production in nanostructural  
53 forms in comparison with other catalysts (A. Ahmad, 2006). It is also stable in aqueous media  
54 (i.e. in both acidic and alkaline solutions). Synthesis of titania nanoparticles can be achieved  
55 using methods such as the chloride process (Kirk et al., 1998), sulphate process (Kirk et al.,  
56 1998), impregnation (Lihitkar et al., 2007), coprecipitation (Sheng et al., 2012), hydrothermal  
57 method (Oh et al., 2006), metal organic chemical vapour deposition methods (Pradhan et al.,  
58 2003), and direct oxidation of  $TiCl_4$  (A. Ahmad, 2006; Yang et al., 2001).

59 Titania exists in three crystalline forms namely rutile, anatase and brookite. The most  
60 important crystalline forms of titania are rutile and anatase. Understanding the factors that  
61 influence the phase stability, for example as a function of particle size, could offer new insights  
62 into how microstructures, relative phase composition and properties of titania-based materials  
63 can be controlled (Zhang and Banfield, 2000). In bulk form, the rutile phase has been found  
64 to be the most stable phase at room temperature (Filyukov et al., 2007), while both anatase and  
65 brookite crystalline are known to be metastable, transforming irreversibly to rutile at high  
66 temperatures (Okeke et al., 2013b). However, phase stability could differ for titania in the  
67 crystalline and at nano particle scale (Koparde and Cummings, 2008). The thermodynamic  
68 stability observed in nanocrystalline rutile and anatase is dependent on the particle-size. As  
69 the size decreases, anatase could attain more stable shape than rutile (Zhang and F. Banfield,  
70 1998) at room temperature and hence the structural characteristics of particles at small scales  
71 is important to understand using advanced simulations. This may be the reason why anatase is  
72 usually synthesized at ultrafine particle-sizes (Naicker et al., 2005). However, thermal stability  
73 characteristics such as melting transition temperature of titania is not yet well studied as a

74 function of phase especially using MD simulations, an aspect addressed in the present work.  
75 Research has shown that a synergy between the two important phases (i.e. anatase and rutile)  
76 can greatly influence certain properties of titania such as its photocatalytic properties as the  
77 two phases possess different physical properties at nanoscale (Filyukov et al., 2007).  
78 Controlling these crystal phases and their morphology is necessary to make them best suited  
79 for the desired application. Furthermore, surface properties of nanoparticles including surface  
80 energy are known to play an important role in influencing the interaction of particles and the  
81 mechanisms that underpin, for example, particle aggregation influences thermal enhancements  
82 in nanofluids (Okeke et al., 2011). Such information is not yet well known for different phases  
83 of tiania as a function of temperature. This aspect is also addressed in the present work.

84 Molecular dynamics (MD) simulation (Cai et al., 2008) is used in this study to investigate  
85 thermo-physical properties of anatase and rutile  $\text{TiO}_2$  nanoparticles. Simulations were  
86 performed for initially spherical particles with diameter ranging from 2 to 6 nm and for  
87 different temperatures in the range from 300 to 3000 K. Thermodynamic and structural  
88 properties, including radial distribution functions and surface energy for anatase and rutile  
89 polymorphs are reported for different particle sizes as a function of temperature.

90 This paper is organized as follows. Section two provides the simulation details including a  
91 description of the force field and molecular dynamics simulation package used. In section  
92 three, simulation results on a fundamental level are presented for the thermodynamic, structural  
93 and surface energy characteristics of anatase and rutile  $\text{TiO}_2$  nanoparticles. The results are  
94 compared for both polymorphs and important information extracted. Finally, the present work  
95 and findings are summarised and conclusions drawn in section four.

## 96 **2 Simulation details**

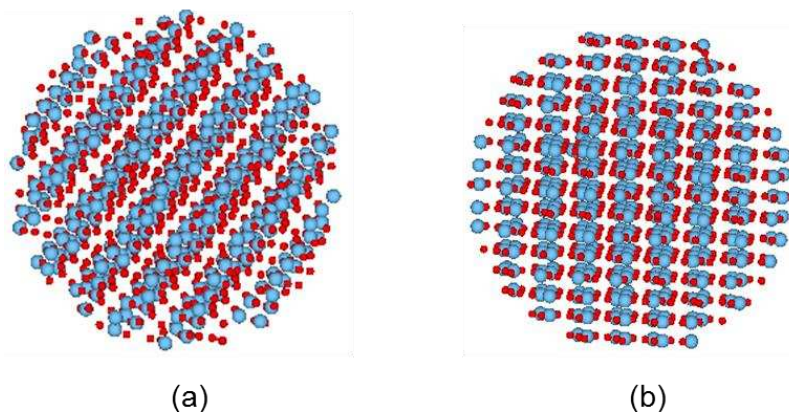
### 97 **2.1 Creation of nanoparticles**

98 The Accelrys Materials Studio 7.0 (Materials Studio suite of crystallographic programs)  
 99 modelling package was used to create TiO<sub>2</sub> nanoparticles of rutile and anatase. Materials  
 100 Studio is a molecular modelling package used to study and analyze models of structures at the  
 101 atomic scale and provides the ability to build and represent molecular structures with enhanced  
 102 graphics. Particles were constructed by initially creating an atomistic model of a perfect crystal  
 103 lattice, using crystallographic information for rutile and anatase some of which are summarized  
 104 in Table 1 (Naicker et al., 2005; Ahmad and Bhattacharya, 2009; Jagtap et al., 2005).

105 **Table 1** Experimental unit cell parameters and space group for rutile and anatase  
 106 (Naicker et al., 2005; Ahmad and Bhattacharya, 2009; Jagtap et al., 2005)

Phase	Crystal System	Space group	a, Å	b, Å	c, Å
Rutile (Sugiyama and Takéuchi, 1991)	Tetragonal	P42/mnm	4.6344	4.6344	2.9919
Anatase (Horn et al., 1972)	Tetragonal	I41/amd	3.784	3.784	9.514

107 Following this, the atomic coordinates for spherical arrays of atoms representing spherical  
 108 particles of anatase and rutile, with diameters ranging from 2 to 6 nm, were calculated from the  
 109 bulk lattice while excess surface atoms of oxygen and titanium were removed to ensure  
 110 stoichiometric and electrical neutrality of the particles (Fig. 1) (Okeke et al., 2013a; Hummer  
 111 et al., 2009). The choice of excess surface atoms on the spherical particles to be removed was  
 112 to minimise the surface energy in vacuum of the unrelaxed particle. The sizes of the particles  
 113 of anatase and rutile used in this study, and the corresponding number of TiO<sub>2</sub> units are given  
 114 in Table 2.



115  
 116 **Fig. 1** Image of typical structure generated for 3 nm (a) rutile and (b) anatase TiO<sub>2</sub>  
 117 nanoparticle created using Materials Studio. Ti and O atoms are shown in red and blue  
 118 colours respectively

119 **Table 2** Size of nanoparticles (in diameter) and the corresponding number of TiO<sub>2</sub> units  
 120 used for anatase and rutile nanoparticles

Particle size (nm)	Anatase	Rutile
2	122	126
3	415	420
4	992	980
5	1941	1918
6	3335	3304

121

## 122 2.2 Representation of the interatomic interactions

123 The force field used is the one widely reported in the literature for modelling TiO<sub>2</sub> polymorphs.  
 124 Various articles have concluded that the Matsui – Akaogi force field (Koparde and Cummings,  
 125 2005; Filyukov et al., 2007; Koparde and Cummings, 2007; Matsui and Akaogi, 1991) is the  
 126 most suitable for atomistic simulations of bulk titania polymorphs for a wide range of  
 127 temperatures and when compared, outperforms other more complicated force fields (Filyukov  
 128 et al., 2007; Koparde and Cummings, 2007). Whilst being a two-body, rigid-ion potential,  
 129 which is relatively undemanding computationally, the Matsui – Akaogi force field reproduces  
 130 the experimentally determined structures of the titania polymorphs and their order of relative  
 131 stability (Koparde and Cummings, 2007). Its reliability over a range of TiO<sub>2</sub> configurations  
 132 makes it suitable for carrying out molecular dynamics simulations at high temperatures (Collins  
 133 et al., 1996). The mathematical form of the interatomic potential is as follows;

$$U(r_{ij}) = A_{ij} \exp\left(-\frac{r_{ij}}{\rho_{ij}}\right) - \frac{C_{ij}}{r_{ij}^6} + \frac{q_i q_j}{r_{ij}} \quad (1)$$

134

135 Outside the scope of the current work, we also performed simulations by refitting the Matsui –  
 136 Akaogi using additional structural data, in the form of elastic constant values, derived from  
 137 DFT calculations carried out using CASTEP. The predictions of the properties from the refined  
 138 force field (derived from fitting) were within reasonable limits with those predicted using the  
 139 classical Matsui-Akaogi force field as well as experiments and DFT calculations from literature  
 140 (Lazzeri et al., 2001; Isaak et al., 1998). Hence, for simplicity, we used Matsui-Akaogi force  
 141 field in the current simulations.

142 For the site–site pairwise interaction  $U(r_{ij})$  is the interaction energy,  $r_{ij}$  is the distance  
 143 between sites  $i$  and  $j$ . The Ti and O atoms are assigned partial charges ( $q$ ) of +2.196 and -1.098  
 144 respectively. The parameters  $A_{ij}$ ,  $\rho_{ij}$  and  $C_{ij}$  are given in Table 3 (Oliver et al., 1997);

145 **Table 3** Potential parameters for TiO<sub>2</sub>. (Oliver et al., 1997)

Interaction	$A_{ij}$ / eV	$\rho_{ij}$ / Å	$C_{ij}$ / eV Å <sup>6</sup>
Ti - O	16957.53	0.194	12.59
Ti - Ti	31120.2	0.154	5.25
O - O	11782.76	0.234	30.22

146

147 Simulations were carried out for water molecules around TiO<sub>2</sub> nanoparticles using the three-  
 148 site SPC/E (extended simple point charge) water potential (Mark and Nilsson, 2001; Okeke et  
 149 al., 2012). The potential has one negatively charged site ( $q_{OW} = -0.8476$ ) representing the O  
 150 atoms, and two positively charged sites ( $q_{HW} = +0.4238$ ) representing the H atoms (Mark and  
 151 Nilsson, 2001). It can be represented in the form of Lennard Jones (LJ) potential as;

$$U(\mathbf{r}_{ij}) = \epsilon_{ij} \left[ \left( \frac{\sigma_{ij}}{r_{ij}} \right)^{12} - 2 \left( \frac{\sigma_{ij}}{r_{ij}} \right)^6 \right] + \frac{q_i q_j}{r_{ij}} \quad (2)$$



152 Where  $\sigma_{ij}$  is the distance at which the potential has its minimum value of  $-\varepsilon_{ij}$ . The values of the  
 153 parameters that correspond to the expression in Equation 2 are shown in Table 4. Interactions  
 154 between the water molecules and TiO<sub>2</sub> nanoparticles were modeled using the interaction  
 155 parameters (Table 4) of Bandura and Kubicki derived from ab initio calculations (Bandura and  
 156 Kubicki, 2003)

157

158 **Table 4** Potential parameters for SPC/E water and interaction between water molecules  
 159 and TiO<sub>2</sub> nanoparticle interactions (Bandura and Kubicki, 2003; Mark and Nilsson, 2001)

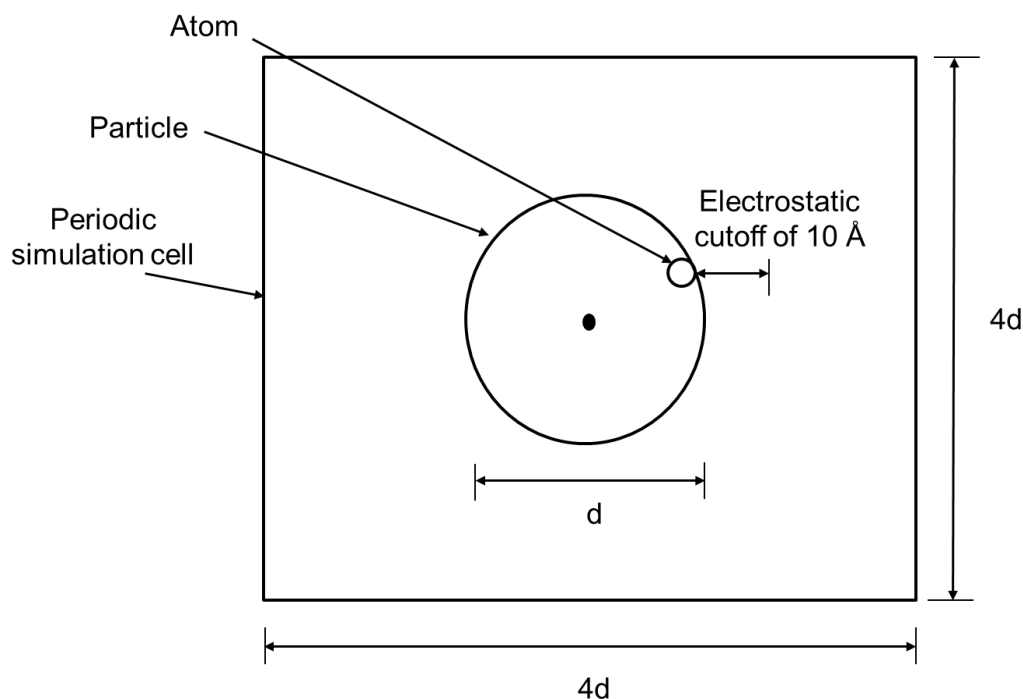
Interaction	$\varepsilon_{ij} / \text{eV}$	$\sigma_{ij} / \text{\AA}$	$C_{ij} / \text{eV \AA}^6$
OW - OW	0.006738	3.166	N/A
OW - HW	0.000	0.000	
HW - HW	0.000	0.000	
Ti - OW	1239.911	0.265	6.4178

160

### 161 2.3 Molecular Dynamics simulation methodology

162 DL\_POLY version 2, a classical molecular dynamics code (Koparde and Cummings, 2005;  
 163 Collins et al., 1996; Alimohammadi and Fichthorn, 2009) was used to carry out the present  
 164 molecular dynamics simulations. The Verlet leapfrog algorithm within DL\_POLY was used  
 165 to integrate Newton's equations of motion and the system temperature was maintained using  
 166 the Berendsen thermostat (Smith et al., 2010). Furthermore, simulations were carried out in  
 167 the canonical ensemble (NVT). The periodic, cubic simulation box used had a size that was at  
 168 least 4 times larger than the diameter of the particle (Fig. 2). This was the case for all  
 169 simulations and was large enough to prevent interactions between the particle and its images  
 170 in the adjoining cells similar to that in a non-periodic boundary system. Simulations were  
 171 carried out for 1 ns, sufficiently long to achieve a steady state in the atomic structure of the  
 172 particles for a given phase. A time step of 1 fs was used in the simulations. The Ewald  
 173 summation technique, as described in the DL\_POLY manual (Smith et al., 2010) for molecular

174 simulations under periodic boundary conditions, was used in calculating the electrostatics  
175 interactions. In terms of short range interactions, a cut-off of  $10\text{\AA}$  was specified (Naicker et  
176 al., 2005), excluding all atoms outside this region including those in periodic images. In this  
177 work, size of the nanoparticles refers to their initial diameter (before simulation). Additionally,  
178 we also performed the MD simulations under non-periodic boundary conditions to make sure  
179 that the simulated generic results are not affected, significantly due to boundary condition.  
180 Unless mentioned otherwise, the simulation results reported here pertain to periodic boundary  
181 condition. In this study, temperature in the non-periodic system was maintained using the  
182 Berendsen thermostat. The electrostatic forces were calculated using the direct Coulomb  
183 summation potential.



184  
185 **Fig. 2** Schematic diagram of a periodic simulation cell with size  $4d$  containing a nanoparticle  
186 of size  $d$

187 Prior to simulations, structural optimization to obtain the minimum energy structure/local  
188 minimum, was initially carried using General Utility Lattice Program (GULP) (Gale and Rohl,

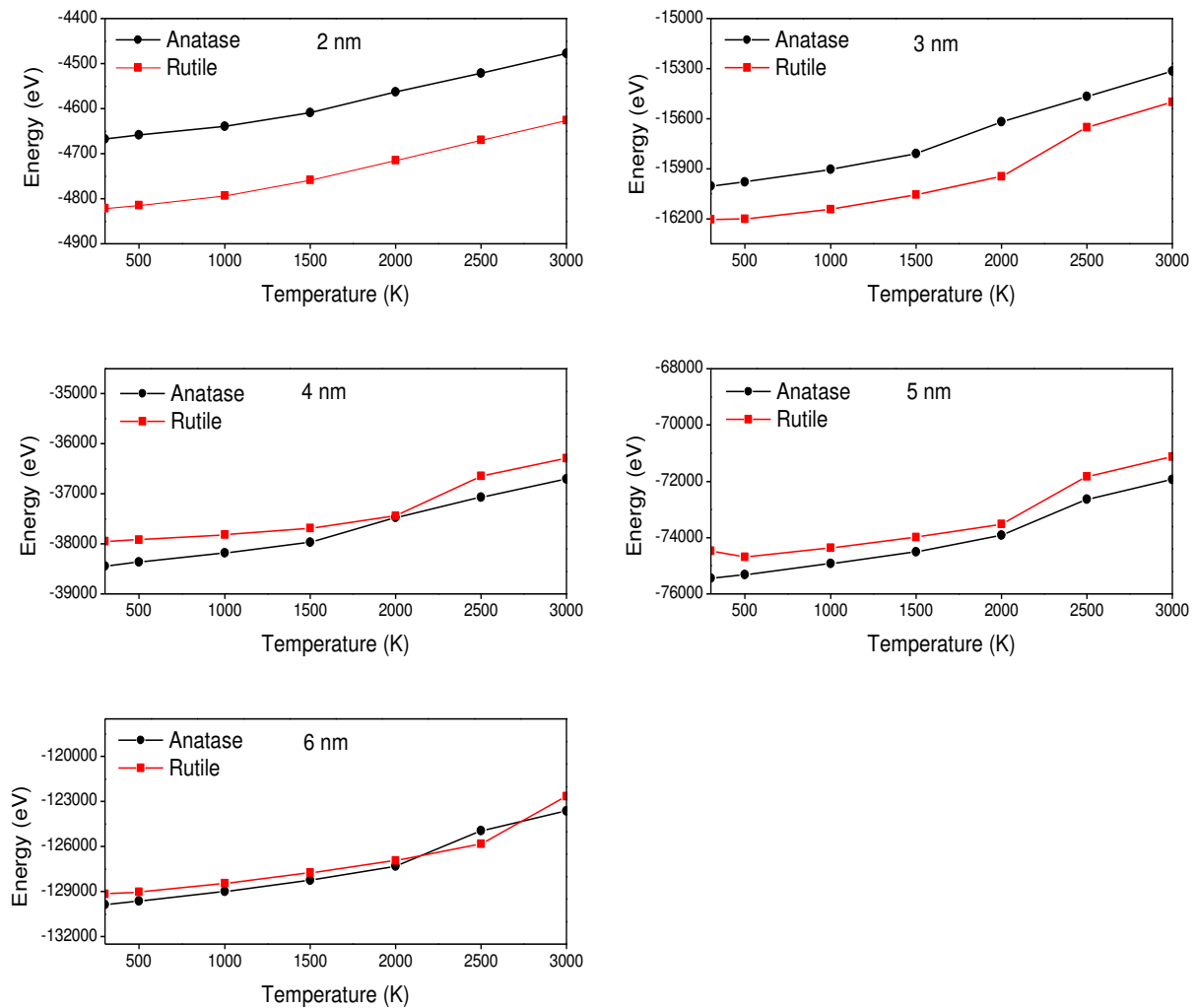
189 2003) for energy calculations of TiO<sub>2</sub> crystals, and DL\_POLY, for energy calculations of TiO<sub>2</sub>  
190 nanoparticles using the force fields (Hummer et al., 2013).

### 191 **3 Results and discussion**

#### 192 **3.1 Thermodynamic properties**

193 The variation of potential energy of the system, with temperature for different nanoparticle  
194 sizes is shown in Fig. 3. An increase in potential energy with temperature can be observed  
195 across all particle sizes. The temperature dependence of the potential energy can be used to  
196 estimate the melting point of TiO<sub>2</sub> rutile and anatase nanoparticles. Filyukov et al.,(Filyukov  
197 et al., 2007) and Collins et al.,(Collins et al., 1996) have used total energy profiles to estimate  
198 the melting point and phase transition temperature of titanium dioxide microclusters of 1011  
199 and 1245 atoms respectively. The number of atoms used in their work corresponds to a particle  
200 diameter of about 3 nm. Filyukov et al, (Filyukov et al., 2007) estimated from their calculations  
201 that the melting point for rutile and anatase is 2450 and 2250 K respectively, while Collins et  
202 al, (Collins et al., 1996) estimated that the melting point for rutile clusters was in the range  
203 from 2150 to 2300 K. In Fig. 3, the rate of change of potential energy with temperature for  
204 both rutile and anatase is seen to increase linearly with increasing temperature for all particle  
205 sizes. Apart from the case of a particle diameter of 2 nm, this trend is seen to be associated  
206 with a sudden steep increase in the rate of change of potential energy at a particular  
207 temperature, which represents the melting transition. The melting transition is characterised  
208 by a temperature range with bounds which can be considered as lower and upper bounds.  
209 Following the sudden steep increase in the rate of change of potential energy for a temperature  
210 range which represents the melting transition, the energy increases linearly with a decreasing  
211 rate. It can also be observed that generally, anatase melts at a lower temperature except for 2  
212 nm particle sizes, compared to rutile. In the case of 3 and 4 nm, the change in energy gradient

213 associated with the melting transition is seen to occur between a temperature of 1500 and 2000  
214 K for anatase, and 2000 and 2500 K for rutile. For 5 nm, this transition is seen to occur between  
215 2000 and 2500 K for both rutile and anatase. However, for 6 nm, the transition is seen to occur  
216 between a temperature of 2000 and 2500 K for anatase, and 2500 and 3000 K for rutile. It can  
217 be further observed that the temperature associated with the melting transition increases with  
218 increasing particle size. Takagi, (Takagi, 1954) was the first to study the size dependence of  
219 very small particles of tin on melting, through experiments (Skripov et al., 1981). Takagi  
220 detected the melting of thin layers of tin using the reflection electron diffraction technique and  
221 took the radii of the spherical tin particles in the layers to be equal to the mean thickness of the  
222 layers (Wronski, 1967). Takagi observed that the melting points of the small particles ranging  
223 from 10 to 1000 Å were lower than those of bulk metals. Following this observation, he  
224 calculated the melting temperature as a function of crystal size, and found that experimental  
225 results were in fairly good agreement with the results from calculations. The size effect of  
226 TiO<sub>2</sub> nanoparticles on their melting temperature has also been investigated theoretically by  
227 Mishra et al, (Mishra et al., 2012) using Arrhenius relation and Lindemann's criteria assuming  
228 that the melting point of the nanoparticles decreases with decrease in size of the nanoparticles,  
229 as evident from the current MD simulations. Though their theoretical analysis accounted for  
230 the size effects of titania nanoparticles, the phase effects were not accounted explicitly unlike  
231 in the current MD simulations.



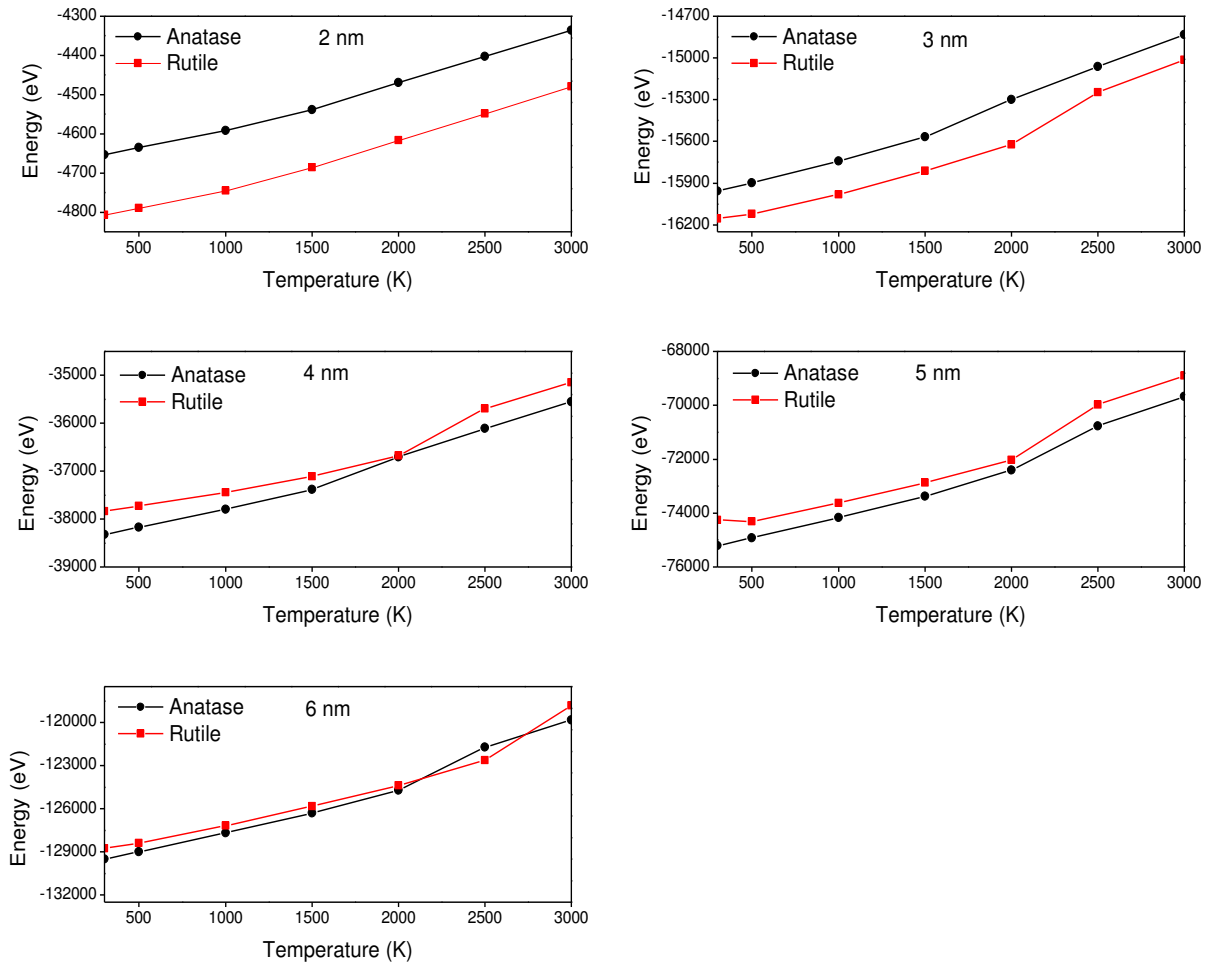
232

233 **Fig. 3** Potential energy as a function of temperature for 2 – 6 nm size nanoparticles for  
 234 simulation in periodic boundary condition

235 We also observed that the potential energy change associated with the melting transition for  
 236 anatase seems to be less than for rutile nanoparticles. This suggests that for nanoparticles of  
 237 the current size range, rutile is the more thermal stable phase as its melting transition occurs  
 238 at higher temperatures compared to anatase.

239 To further confirm our system was similar to that of a non-periodic system, some test  
 240 simulations were conducted and thermodynamic results (Fig. 4) for both systems compared. It  
 241 can be observed the variation of potential energy with temperature in both systems, is fairly  
 242 similar across all particle sizes. Hence, this established a basis to conduct simulations in non-

243 periodic condition, in this study. For brevity, hereafter we present the results pertaining to  
 244 periodic boundary conditions.



245  
 246 **Fig. 4** Potential energy as a function of temperature for 2 – 6 nm size nanoparticles for  
 247 simulation in non-periodic boundary condition

### 248 3.2 Structural properties

249 Radial distribution functions (RDFs) describe the variation of atomic density as a function of  
 250 the distance from a reference atom and therefore represent the structure of liquid and solid  
 251 phases (Brostow, 1977). They are useful for describing the time-averaged, local coordination  
 252 around a specific atom-type and are indicative of a material’s internal structure. The function  
 253  $G(r)$ , represents the probability of locating an atom at a distance  $r$  from a reference atom (in  
 254 our case the centre atom of the particle), compared to a homogenous material such as an ideal

255 gas, of the same number density. The function  $G(r)$  can be used to estimate the coordination  
 256 number  $n_{ij}(r)$  for specific atomic-sites in a structure (Brostow, 1977). The coordination  
 257 number of a central/reference atom represents the number of its nearest neighbours which, as  
 258 a structural parameter, is used in structural analysis. As this number captures the number of  
 259 nearest neighbour atoms bonded to a central atom, it is also associated to the bond length. The  
 260 coordination number,  $n_{ij}(r)$  is given by the following equation (Brostow, 1977);

$$n_{ij}(r) = 4\pi\rho \int_{r_{min}}^{r_{max}} r^2 G(r) dr \quad (3)$$

261 Where  $\rho$  is the number density and is given as;  $\rho = N/V$  in which case  $N$  is the number of  
 262 atoms/molecules in a system of volume  $V$ .

263 Typical RDF plots for 3 nm anatase and rutile are shown for Ti – Ti, Ti – O and O – O pairs at  
 264 temperatures between 300 and 3000 K are shown in Fig. 5 and 6. For the purpose of  
 265 determining the coordination number of Ti atoms, a cut-off radius, which describes the number  
 266 of oxygen atoms in the cut-off region, was set to 2.3 Å. In the context of the RDF plot, the cut-  
 267 off radius represents the position of the first minimum after the first peak ( $r_{min}$  is the lower  
 268 limit before the first peak and  $r_{max}$  is the upper limit after the first peak) (Hines et al., 1985;  
 269 Brostow, 1977). Based on this, the coordination numbers of Ti for the different particle sizes  
 270 and temperatures are reported in Table 5.

271 **Table 5** Coordination number for corresponding particle size, initial bond length  
 272 (before simulation),  $r_{ij}$ , and temperature for anatase and rutile TiO<sub>2</sub> nanoparticles (Okeke et  
 273 al., 2013b)

Anatase								
Particle size (nm)	$r_{ij}$ (Å)	$n_{ij}(r)$						
		Mostly ordered state				Transition state		Liquid state
	Ti - O	300 K	500 K	1000 K	1500 K	2000 K	2500 K	3000 K
2	1.89	5.33	5.31	5.22	5.01	4.78	4.58	4.38
3	1.91	5.48	5.48	5.41	5.27	4.96	4.72	4.50
4	1.91	5.62	5.60	5.53	5.42	5.06	4.79	4.56

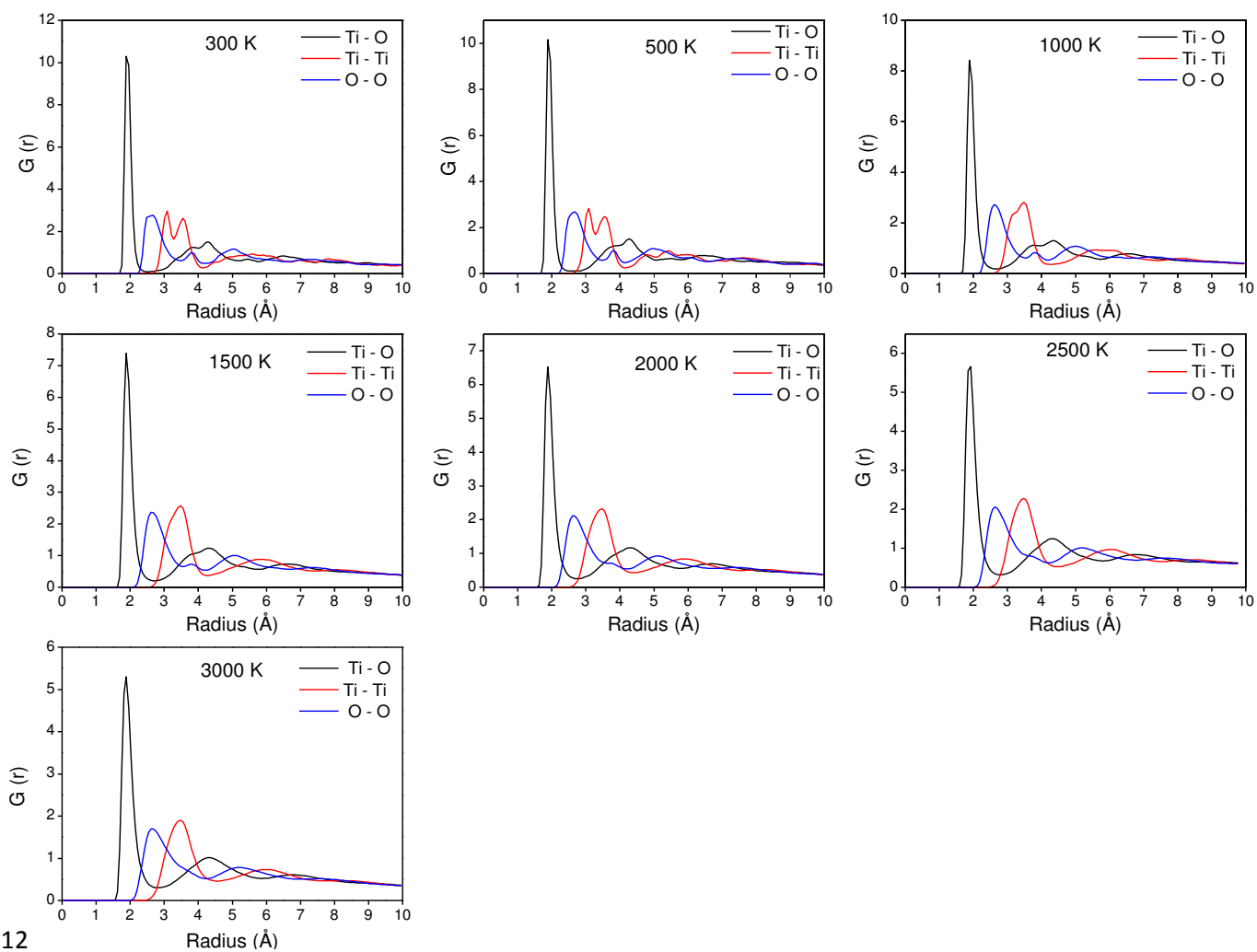
5	1.91	5.68	5.68	5.61	5.52	5.32	4.83	4.60
6	1.91	5.72	5.72	5.67	5.58	5.40	4.85	4.61
Rutile								
Particle size (nm)	$r_{ij}$ (Å)	$n_{ij}(r)$						
		Mostly ordered state				Transition state		Liquid state
	Ti - O	300 K	500 K	1000 K	1500 K	2000 K	2500 K	3000 K
2	1.89	5.31	5.38	5.24	5.11	4.88	4.69	4.50
3	1.91	5.61	5.54	5.43	5.37	5.17	4.72	4.50
4	1.91	5.91	5.62	5.56	5.50	5.36	4.82	4.59
5	1.91	5.69	5.68	5.64	5.60	5.48	5.24	4.70
6	1.91	5.74	5.72	5.69	5.62	5.49	5.26	4.79

274 Table 5 also provides the bond length for both anatase and rutile nanoparticles of 1.89 Å for 2  
275 nm particle size while a bond length of 1.91 Å is seen for particle sizes between 3 and 6 nm  
276 (Naicker et al., 2005). These results are consistent with molecular dynamics simulation results  
277 reported in the literature (Naicker et al., 2005) which suggest that 5-coordinated titanium has  
278 an associated bond length of 1.92 Å. The RDF at 3000 K best describes a molten TiO<sub>2</sub> system.  
279 The melting point of rutile and anatase titania, is 2450 and 2250 K respectively, widely reported  
280 in literature (Collins et al., 1996; Filyukov et al., 2007) falls within the high temperature region  
281 in Table 5, where the coordination number is seen to drop from 5 to 4 (indicating under-  
282 coordination) especially at smaller particle sizes. The bond length for Ti – O in anatase  
283 observed here is in agreement with previous studies (Tang et al., 1993; Zhang et al., 2008;  
284 Banfield et al., 1993) in which a coordination number of 5.3 is reported which suggests a  
285 mixture of Ti – O octahedra and pentahedra having coordination numbers of 6 and 5  
286 respectively. It can be observed from Table 5 that the system becomes tetrahedrally  
287 coordinated (i.e. 4-coordinated titanium) as the temperature increases in transition state, the  
288 coordination number increases with increasing particle size and decreases with increasing  
289 temperature. The tetrahedrally coordinated titanium represents undercoordinated TiO<sub>n</sub> units  
290 (where n < 6) such as those present in Ba<sub>2</sub>TiO<sub>4</sub> where the Ti – O bond length varies between  
291 1.63 and 1.82 Å (Hoang, 2008). This tetrahedral coordination of titanium is thought to  
292 characterise liquid TiO<sub>2</sub> systems (Hoang, 2008). In addition, tetrahedral coordination of



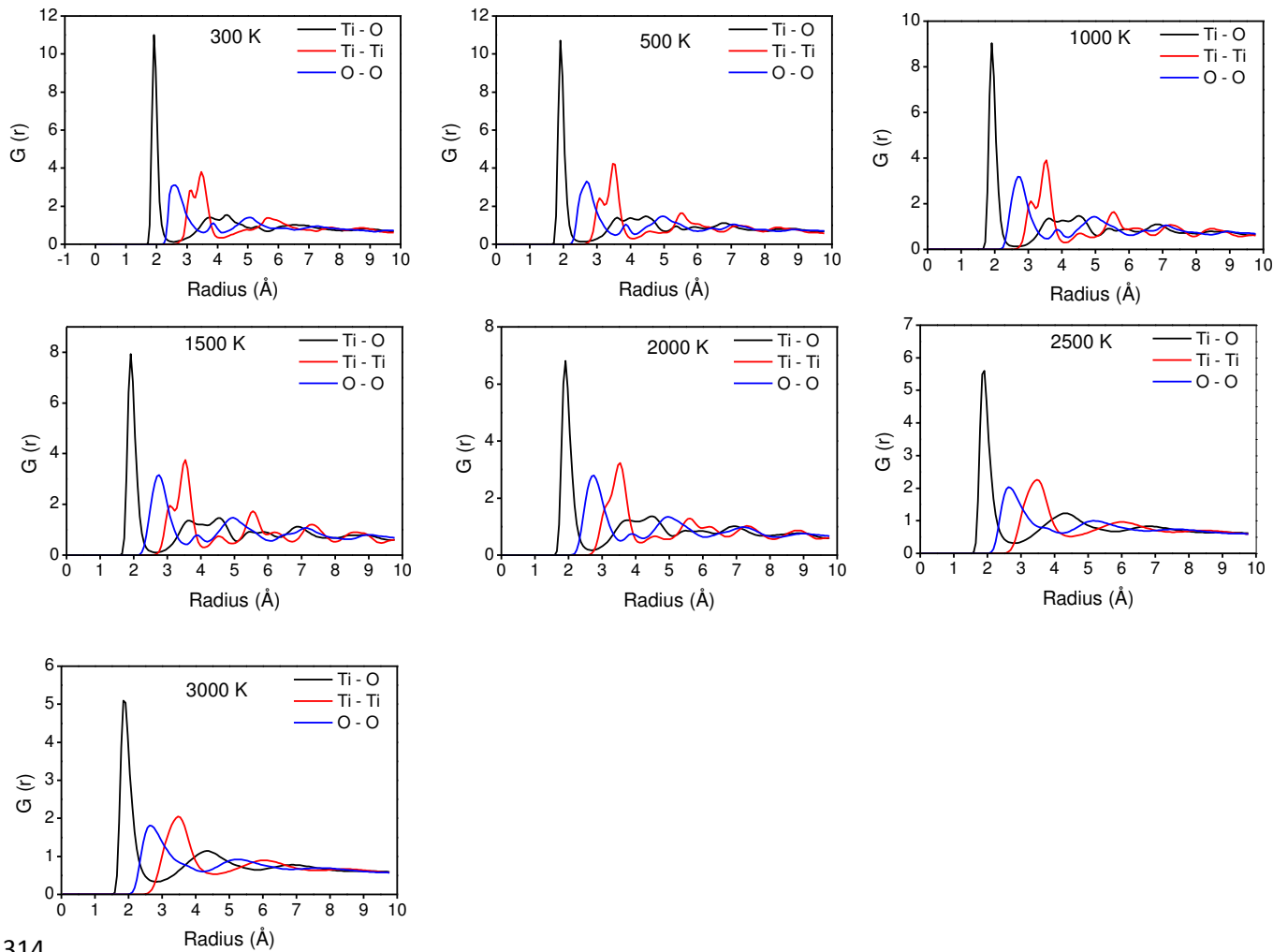
293 titanium is observed in the temperature range from 2000 to 3000 K for all the particle sizes  
294 investigated. These observations correspond to the thermodynamic properties of the anatase  
295 and rutile particles where it is seen that the melting point is approached at temperatures between  
296 2000 and 2500 K after which the system is observed to become more liquid-like.

297 The RDFs in Fig.s 5 - 8 represent a range of structural configurations for anatase and rutile for  
298 typical cases of 3 and 6 nm nanoparticles. For other particle sizes, the generic results were  
299 identical and not repeated here. The RDF's change from well-ordered to molten configuration  
300 for increasing temperature. The well-ordered configuration is characterised by a profile which  
301 manifests a greater number of narrower peaks (for temperatures below 2000 K) with increasing  
302 radius. The molten configuration is characterised by a profile with both fewer and broader  
303 peaks (for temperatures above 2000 K). The plots were generated from the time-average RDF  
304 values over the entire simulation. The greater order, in the case of the lowest temperature (300  
305 K) can be attributed to the higher coordination number of titanium. It is observed that the peaks  
306 for each atom pair broaden as the temperature increases. The initial double peaks observed in  
307 the Ti – Ti and O – O RDF's is seen to broaden as the temperature is increased. Initially at 300  
308 K, the structure is highly crystalline and well ordered. The degree of order decreases with  
309 increase in temperature and the peaks reduce in intensity for high temperatures of 3000 K where  
310 the structure is observed to be more liquid-like. The same general trends were observed for  
311 other particle sizes of this study though not presented here.



312

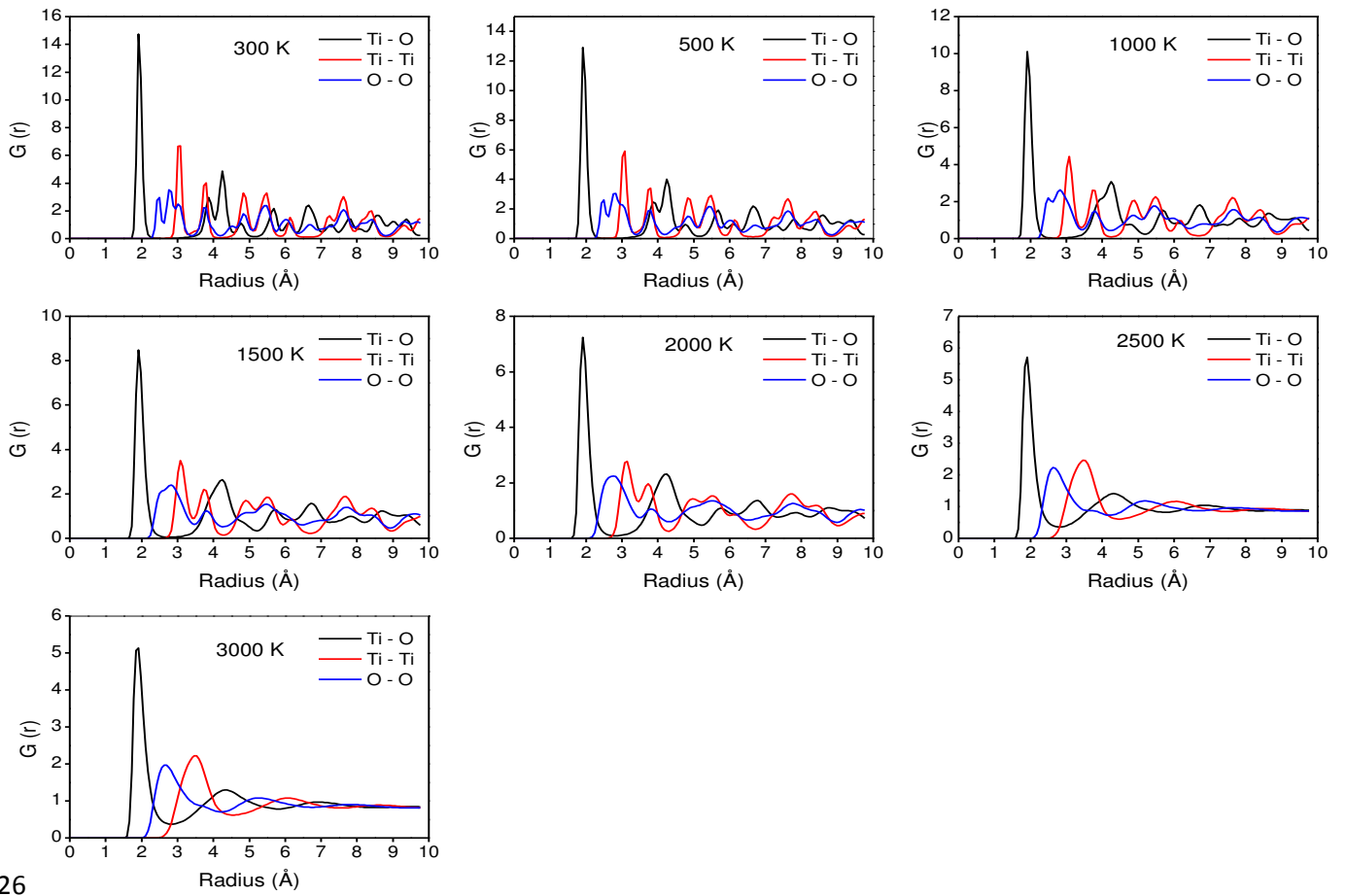
313 **Fig. 5** RDF's for anatase Ti - Ti, Ti - O and O - O pairs for 3 nm



314

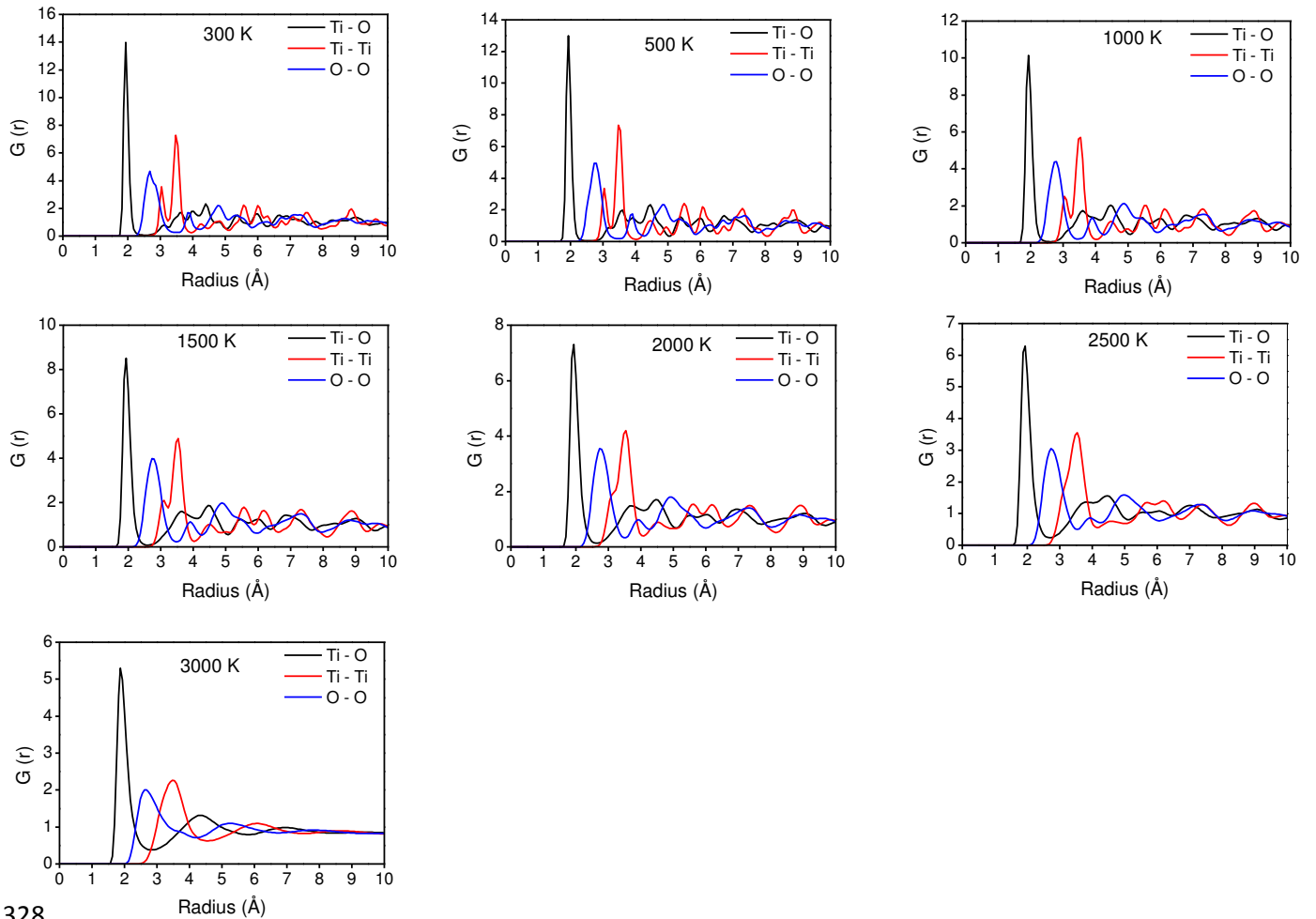
315 **Fig. 6** RDF's for rutile Ti – Ti, Ti – O and O – O pairs for 3 nm

316 The RDF trends for both anatase and rutile can be linked to the variation of potential energy of  
 317 the system with temperature as observed in Fig. 3. In Fig. 3, it can be observed that the change  
 318 in energy gradient associated with the melting transition occurs at almost similar temperatures  
 319 to the temperatures associated with the stretching and broadening of RDF's in Fig. 5 and 6. In  
 320 the case of 3 nm, the melting transition in Fig. 3 occurred between 1500 and 2000 K for anatase,  
 321 and 2000 and 2500 K for rutile, and is similar to the temperature at which the stretching and  
 322 broadening of the RDF's begin to occur, in Fig. 5 and 6. Similarly, for 6 nm, the melting  
 323 transition in Fig. 3 occurred between 2000 and 2500 K for anatase, and at 3000 K for rutile.  
 324 This can be compared to the temperature at which the RDF's begin to stretch in Fig. 7 and 8,  
 325 as stretching begins to occur from 2500 K for anatase, and 3000 K for rutile.



326

327 **Fig. 7** RDF's for anatase Ti - Ti, Ti - O and O - O pairs for 6 nm



328

329 **Fig. 8** RDF's for rutile Ti – Ti, Ti – O and O – O pairs for 6 nm

330 Overall, the temperature (which represents the melting transition) at which the RDF's begin to  
 331 stretch and broaden is observed to be lower for the case of anatase, compared to rutile. This  
 332 further suggests that rutile is the more stable phase for nanoparticles within the size range in  
 333 this study, and is similar to the concluding observations in the preceding thermodynamic  
 334 section.

### 335 3.3 Surface energy

#### 336 3.3.1 TiO<sub>2</sub> crystals

337 Models of crystal morphology are often calculated based on surface energy term which is  
 338 defined in Equation 3, and is taken to represent crystals grown under a minimum driving force  
 339 i.e. at conditions close to thermodynamic equilibrium. Given a bulk energy of  $U_{bulk}$ , an energy

340 for a surface created in the same system,  $U_{surface}$ , and a surface area  $A$ , the surface energy  
 341  $\Delta U_{SE}$  can be defined as(Gale and Rohl, 2003);

$$\Delta U_{SE} = \frac{(U_{surface} - U_{bulk})}{A} \quad (4)$$

342 In this work, surface energy of the crystalline structures of anatase and rutile were obtained  
 343 using the molecular modelling code, GULP (Gale and Rohl, 2003). Furthermore, the center-  
 344 face distances between the center of the crystal and its individual surfaces, were scaled to be  
 345 proportional to the surface energies of the surfaces. Hence, crystal surfaces with low surface  
 346 energies would experience more growth compared to surfaces with high surface energies.

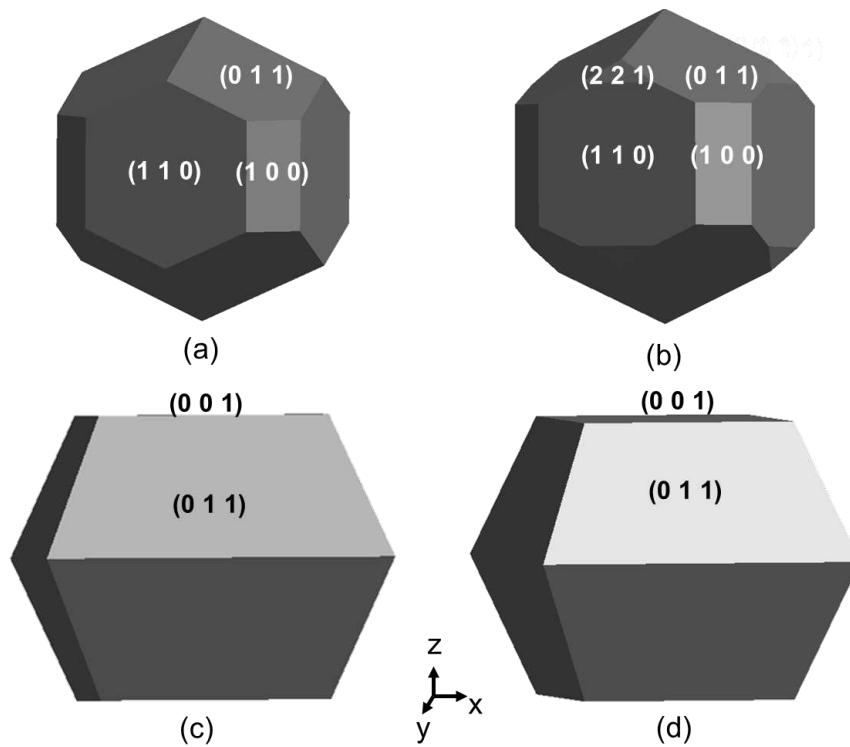
347 Surface energies for anatase and rutile crystals have been reported in Table 6. Similar  
 348 calculations have been previously presented by Oliver et al, (Oliver et al., 1997) for the bulk  
 349 crystals of TiO<sub>2</sub>, which are in a reasonable agreement with the current work. Results show that  
 350 rutile has higher surface energies for both the unrelaxed and relaxed surfaces. For example,  
 351 surface energies for the (0 0 1) and (1 0 0) surfaces of anatase are 1.30 and  
 352 2.28 Jm<sup>-2</sup> respectively, while those for rutile are 2.83 and 4.43 Jm<sup>-2</sup> respectively.

353 **Table 6** Surface energies for rutile and anatase calculated using GULP (0 K)

Surface ( <i>hkl</i> )	Unrelaxed (Jm <sup>-2</sup> )		Relaxed (Jm <sup>-2</sup> )	
	Rutile	Anatase	Rutile	Anatase
(1 1 0)	2.07	2.91	1.79	2.26
(0 1 1)	2.08	1.67	1.86	1.41
(1 0 0)	2.43	2.28	2.10	1.69
(1 2 1)	4.57	-	2.16	-
(0 0 1)	2.83	1.30	2.42	1.30
(2 2 1)	3.77	-	2.12	-
(1 2 0)	-	2.83	-	2.12

354  
 355 Models of the equilibrium crystal morphology for anatase and rutile are presented in Fig. 9,  
 356 and have been predicted using the computed surface energies summarized in Table 6, both at 0

357 K. The (1 1 0), (0 1 1), and (1 0 0) surfaces are expressed in the unrelaxed rutile surfaces. The  
 358 (2 2 1) surface is expressed in the relaxed rutile morphology and is mainly due to the reduction  
 359 in its surface energy upon relaxation from  $3.77 \text{ Jm}^{-2}$  to  $2.12 \text{ Jm}^{-2}$ . The capped octahedral shape  
 360 observed in the anatase morphologies is as a result of the (0 1 1) octahedral form which is  
 361 capped with the (0 0 1) surface. Anatase showed the least change in surface energy when  
 362 comparing the unrelaxed to the relaxed surfaces. It can be observed from Table 6 that the  
 363 amount of change between the unrelaxed and relaxed morphologies is much smaller in the case  
 364 of anatase when compared with that of rutile. This could be attributed to possibly more stability  
 365 of anatase phase in crystalline form (Zhang and F. Banfield, 1998). We wish to point out that  
 366 the surface energy data derived from experiments for rutile and anatase  $\text{TiO}_2$  nanoparticles are  
 367 limited at this time. However, our surface energies for different crystal surfaces were used to  
 368 predict the equilibrium morphology of rutile and anatase. The predicted morphologies (Fig.9)  
 369 are similar to those presented from experiments (Oliver et al., 1997).



370

371 **Fig. 9** Prediction of the calculated equilibrium morphology using surface energies for (a)  
 372 unrelaxed rutile, (b) relaxed rutile, (c) unrelaxed anatase, (d) relaxed anatase

### 373 3.3.2 TiO<sub>2</sub> nanoparticles

374 Surface energy of TiO<sub>2</sub> nanoparticles was calculated using the following expression (Naicker  
375 et al., 2005; Song et al., 2009)

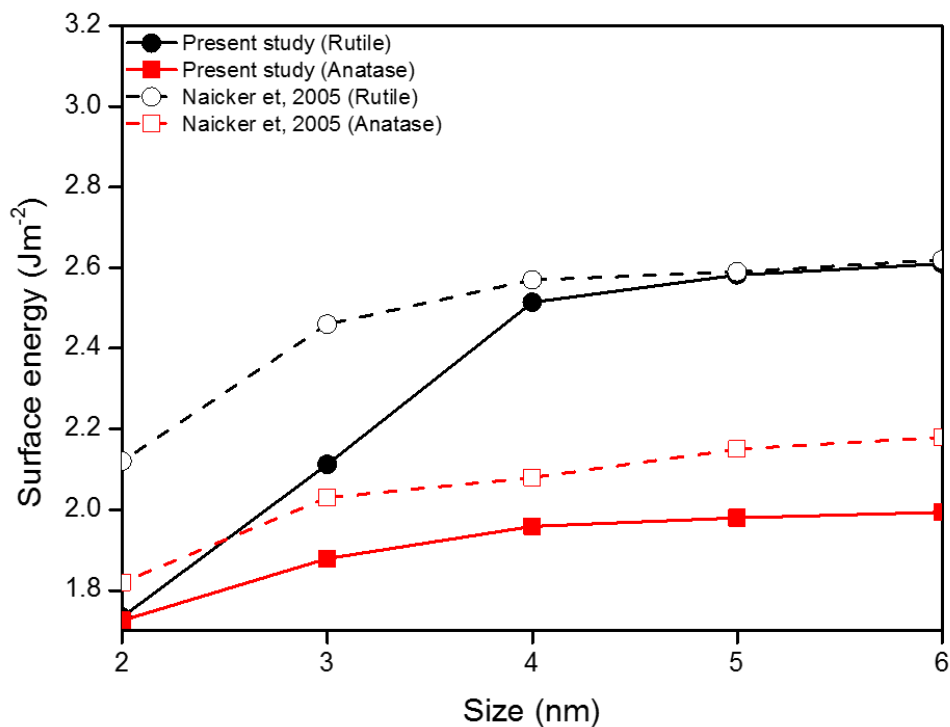
$$\Delta U_{SE} = \frac{(U_{cluster} - nU_{bulk})}{4\pi r^2} \quad (5)$$

376 Where  $U_{cluster}$  is the potential energy of the nanoparticle,  $U_{bulk}$  is the potential energy per  
377 TiO<sub>2</sub> unit in the bulk material,  $n$  is the number of TiO<sub>2</sub> units in the nanoparticle and  $r$  is the  
378 radius of the nanoparticle. The surface energy of nanoparticles is estimated by including any  
379 differences between the energy of atoms in the interior of the nanoparticle, and those in the  
380 crystalline material. Therefore, it is necessary to calculate the energy of the bulk material in  
381 such a way as to minimise any effects due to change in shape of particle surfaces as a result of  
382 these energy differences. In this work, surface energy of the nanoparticles was calculated at  
383 different temperatures ranging from 300 – 2500 K. The energy of the bulk material,  $U_{bulk}$ ,  
384 was calculated at the required temperatures (corresponding to the temperatures employed in  
385 the molecular dynamic simulations) of the nano-particles. Since the particles become less  
386 spherical as temperature increases, the assumption that the particle is spherical and hence the  
387 use of the formula for surface area (i.e.  $4\pi r^2$ ) in Equation 4 becomes a poor approximation.  
388 For this reason, actual surface-area values for the particles were obtained from Materials  
389 Studio. Materials Studio estimates the surface area by creating a Connolly, van der Waals or  
390 solvent surface around the material (treated at the atomic scale), depending on the choice of  
391 surface. In this case, surface area calculations were made using the Connolly surface  
392 (Connolly, 1983).

393 Surface energies of anatase and rutile for different particle sizes at 300 K are reported in Fig.  
394 10. We examined the standard deviations in the potential energies by repeating the simulations

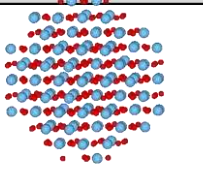
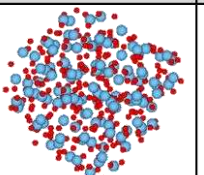
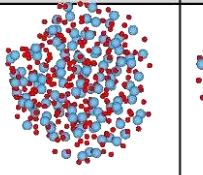
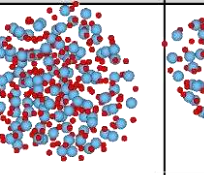
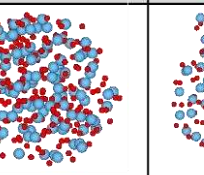
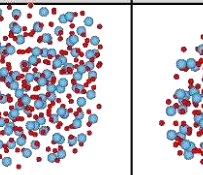
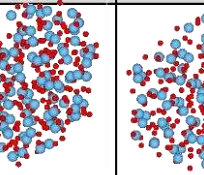
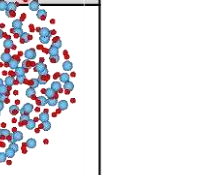
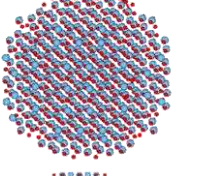
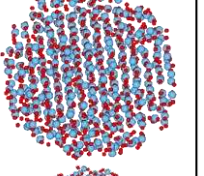
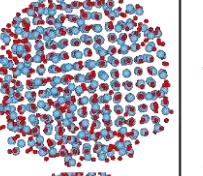
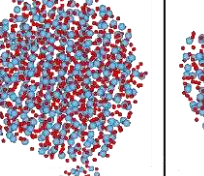
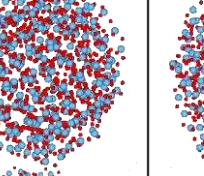
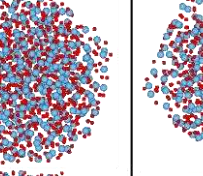
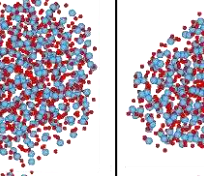
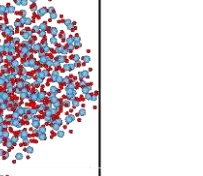

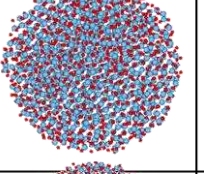
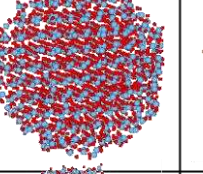
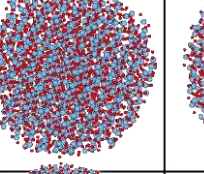
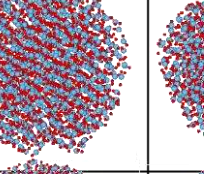
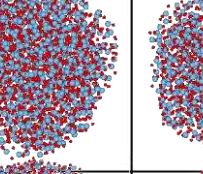
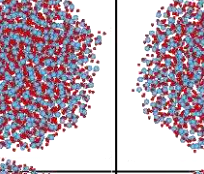
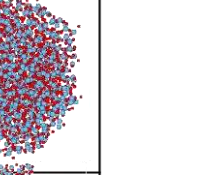
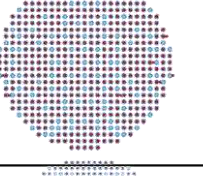
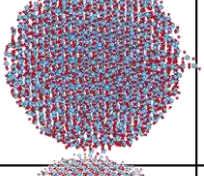
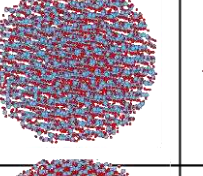
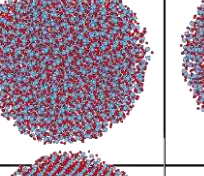
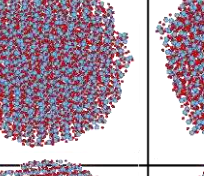
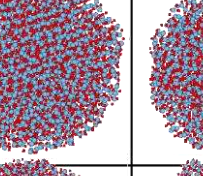
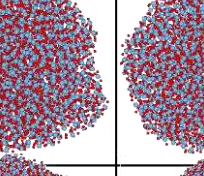
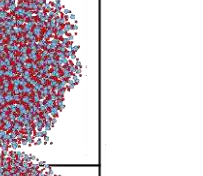
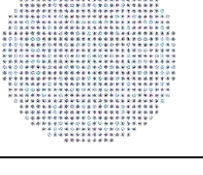
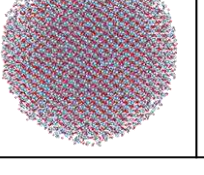
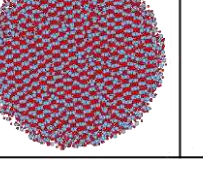
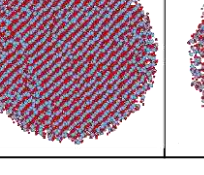
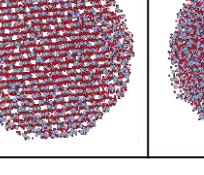
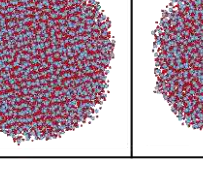
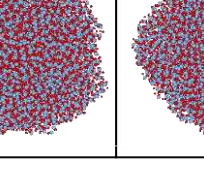
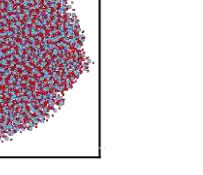


395 3 times and the surface energies were accurate within  $0.02 \text{ Jm}^{-2}$ . This has been further validated  
396 with surface energy data reported by Naicker et al, using MD simulations at 300 K (Naicker et  
397 al., 2005). The plots show that the surface energy of anatase from Naicker et al., (Naicker et  
398 al., 2005) is slightly higher than that found in the present study by about 5 % which is  
399 reasonable given the inherent accuracy of the calculation approach. Surface energy results also  
400 show a significant rise in energy for increasing particle size until a maximum is reached, and  
401 then no further increase is observed. For rutile, the surface energy reported in the literature  
402 (Naicker et al., 2005) for room temperature is higher by about 13 – 16 % between 2 and 4 nm  
403 (Fig. 10). For particles with a diameter greater than 4 nm, the surface energy reported by  
404 Naicker et al. is in reasonable agreement (i.e. surface energy within about 0.3 – 1.2 %). The  
405 observed difference between the data set of Naicker et al.,(Naicker et al., 2005) and the present  
406 study could be due to the fact that their surface energy calculations were based on the  
407 assumption that the nanoparticles remain spherical during simulations as defined by Equation  
408 5. However, by calculating the particle surface-area from the Connolly surface (Connolly,  
409 1983) in the present study, any effect from a change in the shape of the particles, including  
410 faceting, is taken into account.



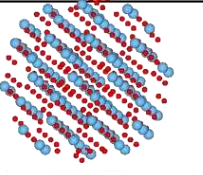
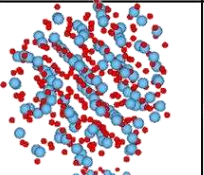
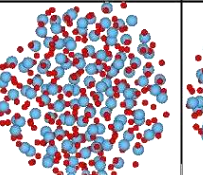
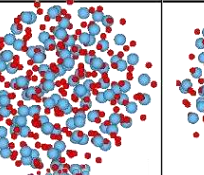
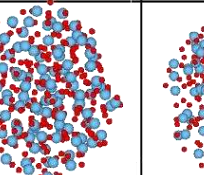
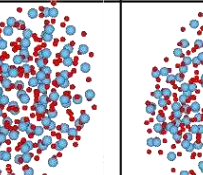
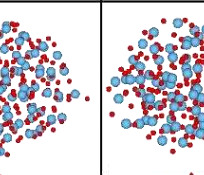
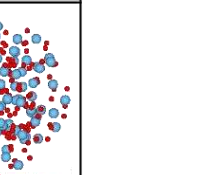
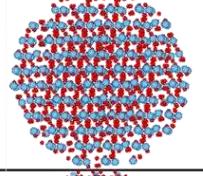
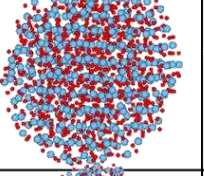
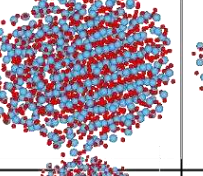
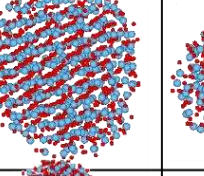
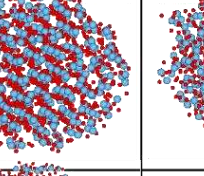
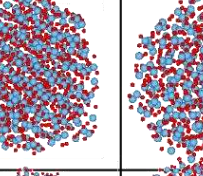
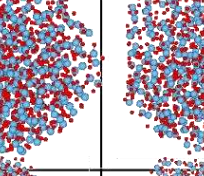
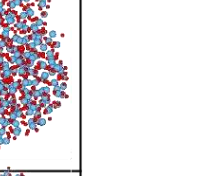
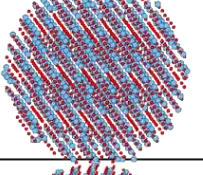
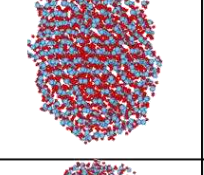
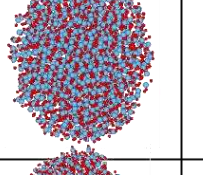
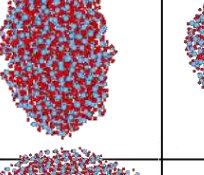
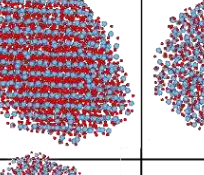
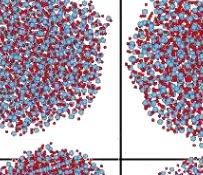
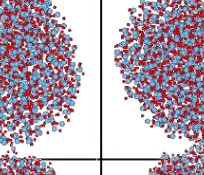
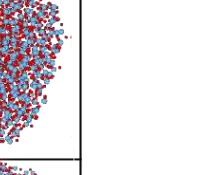
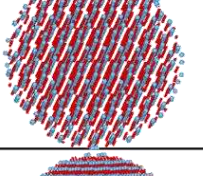
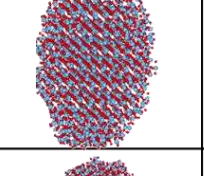
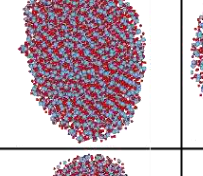
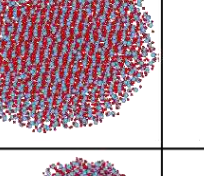
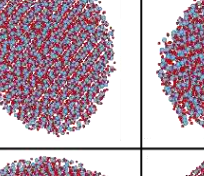
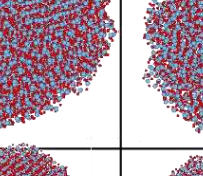
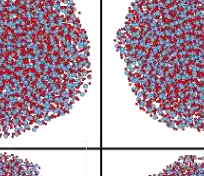
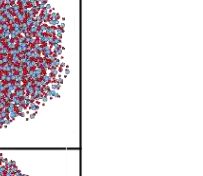
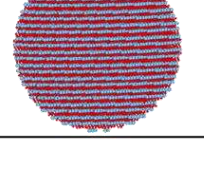
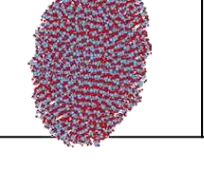
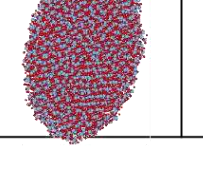
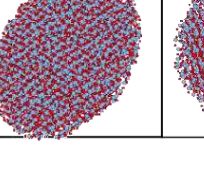
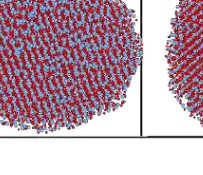
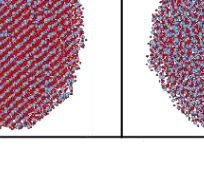
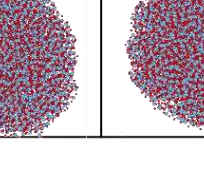
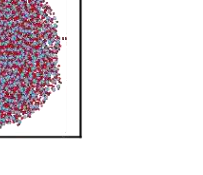
411  
 412 **Fig. 10** Surface energy of anatase and rutile nanoparticles from present study and literature at  
 413 300 K

414 Fig.s 11 and 12 show structural changes in anatase and rutile nanoparticles respectively after  
 415 MD simulations at temperatures between 300 and 3000 K. In the case of anatase, it can be  
 416 seen that the change is more evident for a particle size of 2 nm (top row in Fig. 11), and reduces  
 417 to a minimum for a particle size of 6 nm (bottom row in Fig. 11). The particles tend to retain  
 418 their sphericity more as the particle size increases, especially below the transition temperature  
 419 regime. However, this is not the case with rutile as the particles become non-spherical and  
 420 more oval shaped (as a nanorod) as the particle size increases (Fig. 12).

Size (nm)	Before simulation	Simulations at						
		300 K	500 K	1000 K	1500 K	2000 K	2500 K	3000 K
2								
3								
4								
5								
6								

421

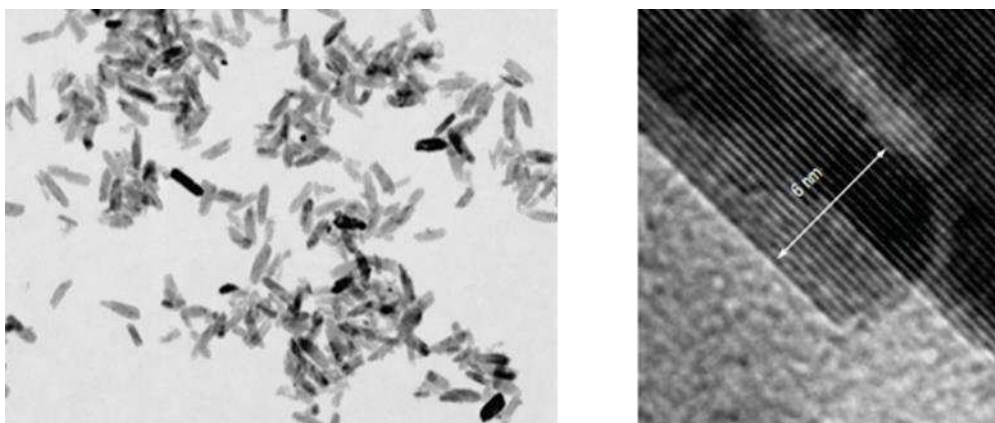
422 **Fig. 11** Structural change of anatase nanoparticles before and after MD simulation at different temperatures. Ti and O atoms in red and blue  
 423 colours respectively

Size (nm)	Before simulation	Simulations at						
		300 K	500 K	1000 K	1500 K	2000 K	2500 K	3000 K
2								
3								
4								
5								
6								

424

425 **Fig. 12** Structural change of rutile nanoparticles before and after MD simulation at different temperatures. Ti and O atoms in red and blue colours  
 426 respectively

427 Notice that 2 and 3 nm rutile nanoparticles in Fig. 12 are still somewhat spherical after  
428 simulation mostly at temperatures between 300 and 1500 K. However, there is a significant  
429 change at particle diameters of 4 to 6 nm as particles tend to become nanorods especially below  
430 the molten temperature. This may be related to the trend in the surface energy plot for rutile in  
431 Fig. 10. A change in the surface energy is observed from 4 nm for increase in particle size.  
432 The increase in surface disordering observed for both anatase and rutile nanoparticles as  
433 temperature increases, is also manifested in the RDF plots of Figures 5 - 8. Reyes-Coronado et  
434 al., (Reyes-Coronado et al., 2008) have experimentally studied anatase and rutile nanoparticles  
435 using TEM, following the hydrothermal treatment of these particles at 200<sup>0</sup>C for a period of  
436 48 hours. They confirmed that upon treatment, the anatase nanoparticles showed a well-faceted  
437 crystal habit. In the case of rutile nanoparticles, they observed that after treatment for a period  
438 of 5 hours at 200<sup>0</sup>C, the particles were seen to organise as nanorods, and oriented to form larger  
439 aggregates in the form of nanorods. The nanorods, showed the (0 1 1) and (1 0 0) surface  
440 planes. Ribeiro et al., (Ribeiro et al., 2007) also carried out characterisation of anatase and  
441 rutile nanoparticles following hydrothermal treatment at 95<sup>0</sup>C for a period of 48 hours. Using  
442 TEM, they observed that while anatase nanoparticles were bipyramidal in shape, the rutile  
443 nanoparticles were rod-like. They also confirm that the (1 1 0) planes are predominant in the  
444 rutile morphology, as a result of their low surface energy. Fig. 13 shows their TEM images of  
445 typical rutile nanorods(Ribeiro et al., 2007). These observations are in line with the shape of  
446 rutile obtained in the current MD simulations as shown in Fig. 12, which takes a rod-like form  
447 at ambient temperature (300 K) and below the melting temperature (transition regime).



448

449 **Fig. 13** TEM images showing rutile TiO<sub>2</sub> nanorods (Ribeiro et al., 2007).

450

451 Interestingly, the observed degree of change of particle shape is less in anatase compared to  
452 rutile (i.e. as seen when comparing Fig. 11 to 12). For example, in the case of 6 nm at 300 K,  
453 the change in sphericity of the anatase particles is about 6 % while that of rutile is about 10 %.

454 It has been reported (Reyes-Coronado et al., 2008) that nanocrystalline rutile tends to grow  
455 mostly in the [1 1 0] direction at elevated temperatures, thereby making the crystals take the  
456 shape of nanorods. The (1 1 0) are the lower energy planes in rutile and show predominance  
457 amongst the other rutile planes, minimizing the total surface energy of the rod. Overall,  
458 observations in Fig.s 11 and 12 suggest that non-spherical TiO<sub>2</sub> particles at the nanoscale in  
459 rutile phase tends to be thermodynamically more stable (also reflected in their RDF's, Fig.s 5  
460 – 8).

461 Surface energy values of TiO<sub>2</sub> nanoparticles at 300 K are shown in Table 7. In both cases of  
462 TiO<sub>2</sub> crystalline and nanoparticles, the surface energy of rutile is seen to be higher than that of  
463 anatase. It can be observed that the surface energy values of both nanoparticle polymorphs are  
464 in reasonable agreement with those of the crystal surfaces presented in Table 6.

465

466

467

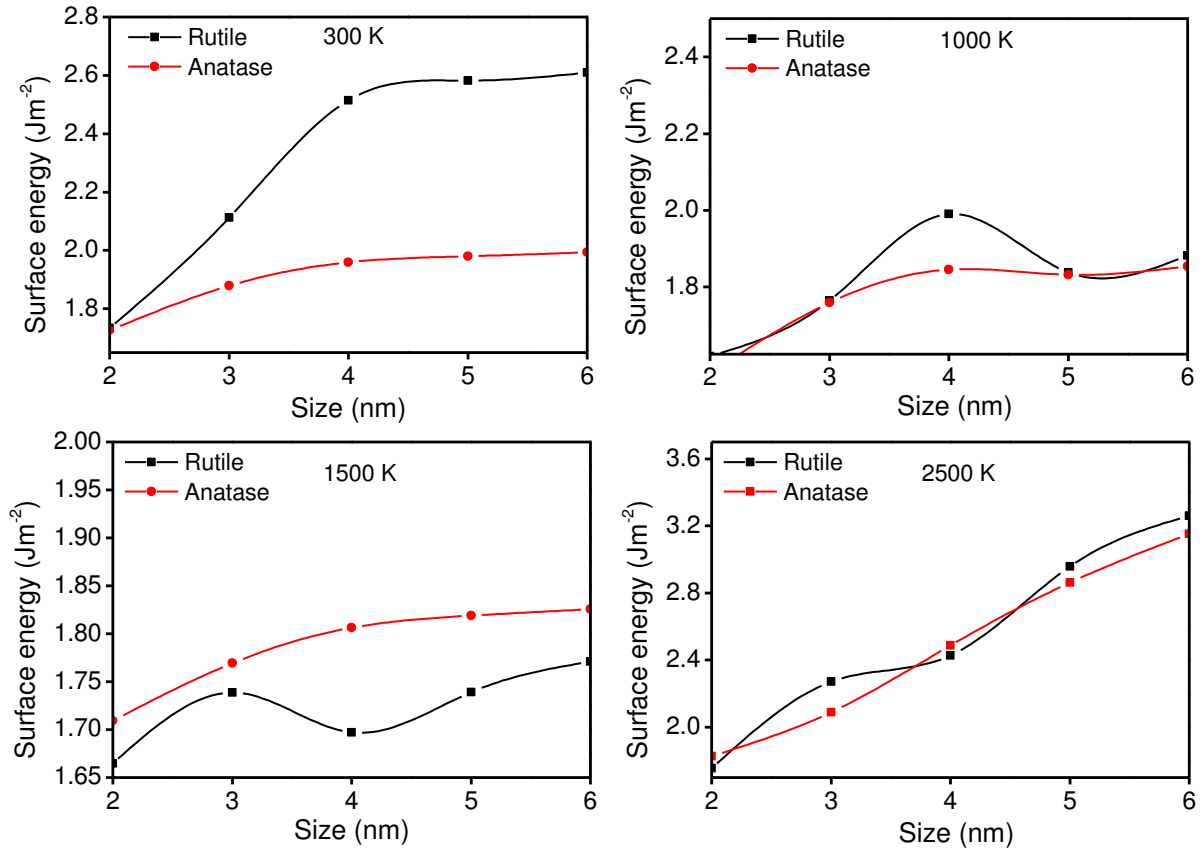
**Table 7** Surface energy (in  $\text{Jm}^{-2}$ ) of rutile and anatase nanoparticles at 300 K

Diameter (nm)	Rutile ( $\text{Jm}^{-2}$ )	Anatase ( $\text{Jm}^{-2}$ )
2	1.73	1.72
3	2.11	1.87
4	2.51	1.95
5	2.58	1.98
6	2.61	1.99

468 The mean surface energy of anatase nanoparticles in the size range between 2 and 6 nm in  
469 diameter is  $1.90 \text{ Jm}^{-2}$  while that for the relaxed crystal surfaces from the present study is  $1.76$   
470  $\text{Jm}^{-2}$ . Similarly, the mean surface energy of rutile nanoparticles between 2 and 6 nm is  $2.28 \text{ Jm}^{-2}$   
471 while that for the crystal surfaces from the present study is  $2.08 \text{ Jm}^{-2}$ . Overall, the surface  
472 energies of rutile and anatase surfaces in Table 5 are within the range of  $1.30$  and  $2.42 \text{ Jm}^{-2}$   
473 with the (1 1 0) and (0 0 1) surfaces having the lowest surface energy for the rutile and anatase  
474 phases, respectively. These surface energy values compare reasonably well with those for the  
475 rutile and anatase nanoparticles. Considering the fact that the crystal surfaces investigated in  
476 this work are the low index surfaces, this suggests that nanoparticles of both rutile and anatase  
477 phases are mostly dominated by low index crystal surfaces. These low index surfaces are  
478 known to be the most stable surfaces (Oliver et al., 1997).

479 Surface energies for anatase and rutile at different temperatures and as a function of particle  
480 size, are reported and compared in Fig. 14. Surface energies for anatase particles at 300, 1000  
481 and 1500 K are seen to increase to a maximum at 4 nm size after which no further significant  
482 increase is observed. It is also worth noting that for particle size at and beyond 4 nm, rutile  
483 nanoparticles are strongly non-spherical in shape. This change in shape is triggered at lower  
484 temperatures in the case of rutile nanoparticles, whereas in anatase, this generally occurs at  
485 higher temperatures.

486



487

488 **Fig. 14** Comparison of surface energy for anatase and rutile nanoparticles at different  
 489 temperatures as a function of particle size

490 The case of surface energy increasing with temperature especially for relatively small anatase  
 491 particle sizes is due to the fact that the nanoparticles start to show signs of faceting with a non-  
 492 spherical shape and become molten as the temperature increases (especially around 2500 K) as  
 493 seen in Fig. 11. This may further mean that the anatase nanoparticles approach the melting  
 494 point and become liquid-like. These observations show that the surface energy contribution to  
 495 thermal properties such as melting point of nanoparticles is significant especially at small  
 496 particle sizes (Naicker et al., 2005). Furthermore, Fig. 14 shows an increase in surface energy  
 497 of rutile nanoparticles for increasing particle sizes, for temperatures 300, 1000 and 1500 K. At  
 498 2500 K, the surface energy of anatase and rutile particles is seen to increase up to a particle  
 499 size of 6 nm. Overall, observations suggest that surface energy directly controls the shape of  
 500 TiO<sub>2</sub> nanoparticles at different temperatures.

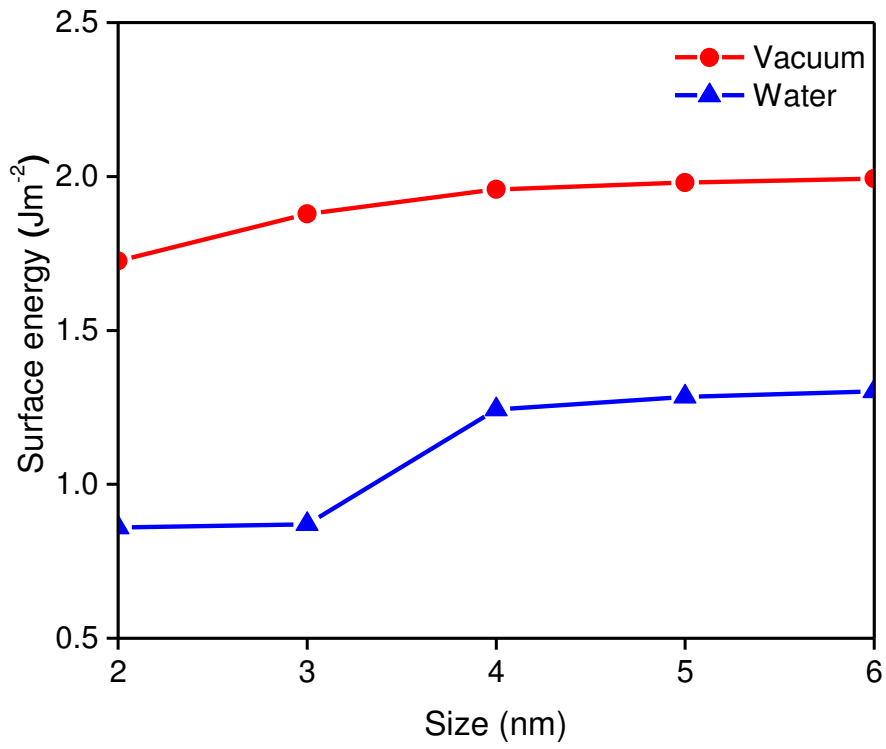


501 **3.3.3 Calculation of surface energy of TiO<sub>2</sub> nanoparticles in water under room temperature**

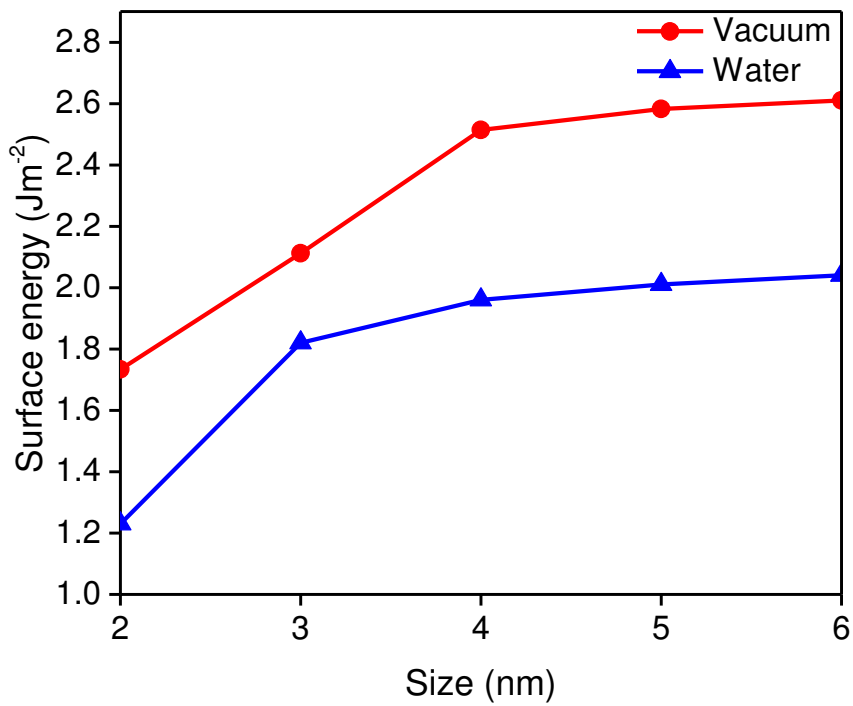
502 Surface energy of the particles in water under 300K was calculated for different particle sizes  
503 ranging from 2–6 nm and phases using the following expression (Okeke et al., 2012);

$$U_{\text{surface}} = \frac{U_{\text{TiO}_2+\text{H}_2\text{O}} - (nU_{\text{bulk}} + U_{\text{H}_2\text{O}})}{A} \quad (6)$$

504 Where  $U_{\text{TiO}_2+\text{H}_2\text{O}}$  is the total energy of the nanoparticle and water together,  $n$  is the number of  
505 TiO<sub>2</sub> molecules,  $U_{\text{H}_2\text{O}}$  is the energy of pure water and  $A$  is the surface area of the nanoparticle.  
506 Results of surface energy for the anatase and rutile nanoparticles in water and vacuum  
507 environments are shown in Fig. 15. Surface energy of anatase and rutile nanoparticles in both  
508 environments is seen to increase significantly with increase in particle size until 4 nm, above  
509 which no significant increase in surface energy is observed. Surface energy of anatase  
510 nanoparticles in vacuum is seen to be higher than that in water by about 50% for the smaller  
511 particles (i.e. 2 and 3nm) and about 35% for the larger particles (i.e. 4 to 6 nm) (Okeke et al.,  
512 2012). These figures for the rutile nanoparticles studied here are about 30% and 20%  
513 respectively. Surface energy of rutile nanoparticles is also seen to be lower in water when  
514 compared to vacuum environment. Similar to our work, Hummer et al. (2013) also observed  
515 higher surface energy for rutile compared to anatase faceted nano particles (of less than 3nm  
516 size) under both vacuum and liquid environments. This could be due to water molecules  
517 binding strongly to the surface of anatase and rutile nanoparticles, thereby relaxing their surface  
518 energy and stabilizing the particles in an aqueous environment (Hummer et al., 2013).



(a)



(b)

519  
520

521  
522

523 **Fig. 15** Surface energy of (a) anatase and (b) rutile TiO<sub>2</sub> nanoparticles in water and vacuum  
524 environments at 300 K

525

## 526 **4 Conclusions**

527 MD simulations were performed for the thermodynamic, structural and surface energy of  
528 anatase and rutile TiO<sub>2</sub> nanoparticles. The variation of potential energy of the system, with  
529 temperature for different nanoparticle sizes, was used to evaluate the melting point of TiO<sub>2</sub>  
530 anatase and rutile nanoparticles. It was observed that the temperature associated with the  
531 melting transition increased with increasing particle size. Here, the potential energy change  
532 associated with the melting transition for anatase was seen to be less than that for rutile  
533 nanoparticles, suggesting that for particle sizes considered in this study, rutile is the most  
534 thermally stable phase. The RDF trends for both anatase and rutile nanoparticles were linked  
535 to the variation of potential energy of the system with temperature. We observed that the  
536 change in energy gradient associated with the melting transition occurred at almost similar  
537 temperatures associated with the stretching and broadening of the RDF's. The temperature  
538 (corresponding to the melting transition) at which the RDF's began to stretch and broaden was  
539 observed to be lower for the case of anatase, which suggests that rutile is the more stable phase  
540 for nanoparticles within the size range in this study. Further observations on the structural  
541 changes in anatase and rutile nanoparticles after MD simulations at different temperatures  
542 revealed that non-spherical, rod-like TiO<sub>2</sub> nanoparticles at the nanoscale in rutile phase tends  
543 to be thermodynamically more stable. This was also reflected in their respective RDF plots.  
544 Results also suggest that surface energy directly controls the shape of TiO<sub>2</sub> nanoparticles at  
545 different temperatures. Surface energy of anatase and rutile nanoparticles in water is seen to  
546 be lower than that in vacuum. The strong binding of water molecules on the surface atoms of  
547 the particles relaxes their surface energy, hence the lower surface energy in water (Hummer et  
548 al 2013). In both environments, surface energy of both anatase and rutile nanoparticles is seen  
549 to increase to a maximum at about 4 nm, after which no further significant increase is observed.

550 Furthermore, information provided in this will give more understanding of such fundamental  
551 properties for developing new applications, for example in the area of thermal enhancement of  
552 nanofluids, which will be presented in future publications. The fundamental properties  
553 presented here could further help to study scaling-up production methodologies of TiO<sub>2</sub>  
554 nanoparticles using multi-scale methodologies in which such basic properties could form as  
555 input to higher level studies.

## 556 **Nomenclature**

$U(r_{ij})$	interaction energy
$r_{ij}$	distance between sites $i$ and $j$
$q$	partial charge
$G(r)$	probability of locating an atom at a distance $r$ from a reference atom compared to a homogenous material of the same number density
$n_{ij}(r)$	coordination number
$\Delta U_{SE}$	surface energy
$A$	surface area
$U_{bulk}$	bulk energy
$U_{cluster}$	potential energy of nanoparticle

## 557 **Greek symbols**

$\rho$	density
--------	---------

558

559

560

561

562

563 **References**

- 564 A. Ahmad, G.H.A., Salman Aziz. 2006. Synthesis and applications of TiO<sub>2</sub> nanoparticles.  
565 Pakistan Engineering Congress, 70th Annual Session Proceedings.
- 566 Ahmad, M.I. and Bhattacharya, S.S. 2009. Size effect on the lattice parameters of  
567 nanocrystalline anatase. *Applied Physics Letters*. **95**(19), pp.191906-191906-3.
- 568 Alimohammadi, M. and Fichthorn, K.A. 2009. Molecular Dynamics Simulation of the  
569 Aggregation of Titanium Dioxide Nanocrystals: Preferential Alignment. *Nano Letters*.  
570 **9**(12), pp.4198-4203.
- 571 Bandura, A.V. and Kubicki, J.D. 2003. Derivation of Force Field Parameters for TiO<sub>2</sub>-H<sub>2</sub>O  
572 Systems from ab Initio Calculations. *The Journal of Physical Chemistry B*. **107**(40),  
573 pp.11072-11081.
- 574 Banfield, J.F.Bischoff, B.L. and Anderson, M.A. 1993. TiO<sub>2</sub> accessory minerals: coarsening,  
575 and transformation kinetics in pure and doped synthetic nanocrystalline materials.  
576 *Chemical Geology*. **110**(1-3), pp.211-231.
- 577 Brostow, W. 1977. Radial distribution function peaks and coordination numbers in liquids  
578 and in amorphous solids. *Chemical Physics Letters*. **49**(2), pp.285-288.
- 579 Cai, Q.Buts, A.Seaton, N.A. and Biggs, M.J. 2008. A pore network model for diffusion in  
580 nanoporous carbons: Validation by molecular dynamics simulation. *Chemical*  
581 *Engineering Science*. **63**(13), pp.3319-3327.
- 582 Chaudhari, G.N.Bambole, D.R.Bodade, A.B. and Padole, P.R. 2006. Characterization of  
583 nanosized TiO<sub>2</sub> based H<sub>2</sub>S gas sensor. *Journal of Materials Science*. **41**(15),  
584 pp.4860-4864.
- 585 Chen, C.-L. and Weng, H.-S. 2005. Nanosized CeO<sub>2</sub>-supported metal oxide catalysts for  
586 catalytic reduction of SO<sub>2</sub> with CO as a reducing agent. *Applied Catalysis B:*  
587 *Environmental*. **55**(2), pp.115-122.
- 588 Collins, D.R.Smith, W.Harrison, N.M. and Forester, T.R. 1996. Molecular dynamics study of  
589 TiO<sub>2</sub> microclusters. *Journal of Materials Chemistry*. **6**(8), pp.1385-1390.
- 590 Connolly, M. 1983. Analytical molecular surface calculation. *Journal of Applied*  
591 *Crystallography*. **16**(5), pp.548-558.
- 592 Filyukov, D.Brodskaya, E.Piotrovskaya, E. and de Leeuw, S. 2007. Molecular-dynamics  
593 simulation of nanoclusters of crystal modifications of titanium dioxide. *Russian*  
594 *Journal of General Chemistry*. **77**(1), pp.10-16.

595 Gale, J. and Rohl, A. 2003. The general utility lattice program (GULP).

596 Haverkamp, R.G. 2010. A Decade of Nanoparticle Research in Australia and New Zealand.

597 Particulate Science and Technology: An International Journal. **28**(1), pp.1 - 40.

598 Hines, A.Walls, H. and Jethani, K. 1985. Determination of the coordination number of liquid

599 metals near the melting point. Metallurgical Transactions A. **16**(1), pp.267-274.

600 Hoang, V.V. 2008. The glass transition and thermodynamics of liquid and amorphous TiO<sub>2</sub>

601 nanoparticles. Nanotechnology. **19**(10), p105706.

602 Horn, M.Schwerdtfeger, C. and Meagher, E. 1972. Refinement of the structure of anatase at

603 several temperatures. Zeitschrift für Kristallographie. **136**(3-4), p273.

604 Hu, J.Q.Ma, X.L.Shang, N.G.Xie, Z.Y.Wong, N.B.Lee, C.S. and Lee, S.T. 2002. Large-Scale

605 Rapid Oxidation Synthesis of SnO<sub>2</sub> Nanoribbons. The Journal of Physical Chemistry

606 B. **106**(15), pp.3823-3826.

607 Hummer, D.R.Kubicki, J.D.Kent, P.R.C. and Heaney, P.J. 2013. Single-Site and Monolayer

608 Surface Hydration Energy of Anatase and Rutile Nanoparticles Using Density

609 Functional Theory. The Journal of Physical Chemistry C. **117**(49), pp.26084-26090.

610 Hummer, D.R.Kubicki, J.D.Kent, P.R.C.Post, J.E. and Heaney, P.J. 2009. Origin of

611 Nanoscale Phase Stability Reversals in Titanium Oxide Polymorphs. The Journal of

612 Physical Chemistry C. **113**(11), pp.4240-4245.

613 Isaak, D.G.Carnes, J.D.Anderson, O.L.Cynn, H. and Hake, E. 1998. Elasticity of TiO<sub>2</sub> rutile

614 to 1800 K. Physics and Chemistry of Minerals. **26**(1), pp.31-43.

615 Jagtap, N.Bhagwat, M.Awati, P. and Ramaswamy, V. 2005. Characterization of

616 nanocrystalline anatase titania: an in situ HTXRD study. Thermochemica Acta. **427**(1-

617 2), pp.37-41.

618 Kermanpur, A.Ghassemali, E. and Salemizadeh, S. 2008. Synthesis and characterisation of

619 microporous titania membranes by dip-coating of anodised alumina substrates using

620 sol-gel method. Journal of Alloys and Compounds. **461**(1-2), pp.331-335.

621 Kirk, R.E.Othmer, D.F.Kroschwitz, J.I. and Howe-Grant, M. 1998. Encyclopedia of chemical

622 technology. John Wiley & Sons.

623 Koparde, V.N. and Cummings, P.T. 2005. Molecular Dynamics Simulation of Titanium

624 Dioxide Nanoparticle Sintering. The Journal of Physical Chemistry B. **109**(51),

625 pp.24280-24287.

626 Koparde, V.N. and Cummings, P.T. 2007. Molecular Dynamics Study of Water Adsorption

627 on TiO<sub>2</sub> Nanoparticles. The Journal of Physical Chemistry C. **111**(19), pp.6920-6926.

628 Koparde, V.N. and Cummings, P.T. 2008. Phase Transformations during Sintering of Titania  
629 Nanoparticles. ACS Nano. **2**(8), pp.1620-1624.

630 Lazzeri, M. Vittadini, A. and Selloni, A. 2001. Structure and energetics of stoichiometric  
631  $\{\mathrm{TiO}\}_2$  anatase surfaces. Physical Review B. **63**(15), p155409.

632 Lihitkar, N.B. Abyaneh, M.K. Samuel, V. Pasricha, R. Gosavi, S.W. and Kulkarni, S.K. 2007.  
633 Titania nanoparticles synthesis in mesoporous molecular sieve MCM-41. Journal of  
634 Colloid and Interface Science. **314**(1), pp.310-316.

635 Mark, P. and Nilsson, L. 2001. Structure and Dynamics of the TIP3P, SPC, and SPC/E Water  
636 Models at 298 K. The Journal of Physical Chemistry A. **105**(43), pp.9954-9960.

637 Materials Studio suite of crystallographic programs. [Online]. Available from:  
638 <http://www.accelrys.com/>.

639 Matsui, M. and Akaogi, M. 1991. Molecular Dynamics Simulation of the Structural and  
640 Physical Properties of the Four Polymorphs of TiO<sub>2</sub>. Molecular Simulation. **6**(4-6),  
641 pp.239-244.

642 Mishra, S. Jha, P. and Pratap, A. 2012. Study of size-dependent glass transition and  
643 Kauzmann temperature of titanium dioxide nanoparticles. Journal of Thermal  
644 Analysis and Calorimetry. **107**(1), pp.65-68.

645 Naicker, P.K. Cummings, P.T. Zhang, H. and Banfield, J.F. 2005. Characterization of  
646 Titanium Dioxide Nanoparticles Using Molecular Dynamics Simulations. The  
647 Journal of Physical Chemistry B. **109**(32), pp.15243-15249.

648 Oh, S.W. Park, S.-H. and Sun, Y.-K. 2006. Hydrothermal synthesis of nano-sized anatase  
649 TiO<sub>2</sub> powders for lithium secondary anode materials. Journal of Power Sources.  
650 **161**(2), pp.1314-1318.

651 Okeke, G. Hammond, R. and Antony, S.J. 2012. Analysis of Structural and Surface Properties  
652 of TiO<sub>2</sub> Nanoparticles in Water and Vacuum Using Molecular Dynamics Modeling  
653 and Simulations. Journal of Nanofluids. **1**(1), pp.21-27.

654 Okeke, G. Hammond, R. and Joseph Antony, S. 2013a. Influence of size and temperature on  
655 the phase stability and thermophysical properties of anatase TiO<sub>2</sub> nanoparticles:  
656 molecular dynamics simulation. Journal of Nanoparticle Research. **15**(4), pp.1-9.

657 Okeke, G. Hammond, R.B. and Antony, S.J. 2013b. Molecular Dynamics Simulation of  
658 Anatase TiO<sub>2</sub> Nanoparticles. Journal of Nanoscience and Nanotechnology. **13**(2),  
659 pp.1047-1052.

660 Okeke, G. Witharana, S. Antony, S. and Ding, Y. 2011. Computational analysis of factors  
661 influencing thermal conductivity of nanofluids. *Journal of Nanoparticle Research*.  
662 **13**(12), pp.6365-6375.

663 Oliver, P.M. Watson, G.W. Toby Kelsey, E. and Parker, S.C. 1997. Atomistic simulation of  
664 the surface structure of the TiO<sub>2</sub> polymorphs rutile and anatase. *Journal of Materials*  
665 *Chemistry*. **7**(3), pp.563-568.

666 Onozuka, K. Ding, B. Tsuge, Y. Naka, T. Yamazaki, M. Sugi, S. Ohno, S. Yoshikawa, M. and  
667 Shiratori, S. 2006. Electrospinning processed nanofibrous TiO<sub>2</sub> membranes for  
668 photovoltaic applications. *Nanotechnology*. **17**(4), p1026.

669 Park, S.-J. Kang, Y.C. Evans, E.A. and Ramsier, R.D. 2010. Physical Characteristics of Titania  
670 Nanofibers Synthesized by Sol-Gel and Electrospinning Techniques. *Journal of*  
671 *Engineered Fibers and Fabrics*.

672 Pradhan, S.K. Reucroft, P.J. Yang, F. and Dozier, A. 2003. Growth of TiO<sub>2</sub> nanorods by  
673 metalorganic chemical vapor deposition. *Journal of Crystal Growth*. **256**(1–2), pp.83-  
674 88.

675 Reyes-Coronado, D. Rodríguez-Gattorno, G. Espinosa-Pesqueira, M.E. Cab, C. Coss, R.d. and  
676 Oskam, G. 2008. Phase-pure TiO<sub>2</sub> nanoparticles: anatase, brookite and rutile.  
677 *Nanotechnology*. **19**(14), p145605.

678 Ribeiro, C. Vila, C. Milton Elias de Matos, J. Bettini, J. Longo, E. and Leite, E.R. 2007. Role of  
679 the Oriented Attachment Mechanism in the Phase Transformation of Oxide  
680 Nanocrystals. *Chemistry – A European Journal*. **13**(20), pp.5798-5803.

681 Sheng, Z. Hu, Y. Xue, J. Wang, X. and Liao, W. 2012. A novel co-precipitation method for  
682 preparation of Mn–Ce/TiO<sub>2</sub> composites for NO<sub>x</sub> reduction with NH<sub>3</sub> at low  
683 temperature. *Environmental Technology*. **33**(21), pp.2421-2428.

684 Skripov, V.P. Koverda, V.P. and Skokov, V.N. 1981. Size effect on melting of small particles.  
685 *physica status solidi (a)*. **66**(1), pp.109-118.

686 Smith, W. Forester, T.R. and Todorov, I.T. 2010. The DL\_POLY\_2 User Manual. STFC  
687 Daresbury Laboratory. **Version 2.21**.

688 Song, D.-P. Liang, Y.-C. Chen, M.-J. and Bai, Q.-S. 2009. Molecular dynamics study on  
689 surface structure and surface energy of rutile TiO<sub>2</sub> (1 1 0). *Applied Surface Science*.  
690 **255**(11), pp.5702-5708.

691 Soo-Jin Park, Y.C.K., Ju Y. Park, Ed A. Evans, Rex D. Ramsier, and George G. Chase. 2010.  
692 Physical Characteristics of Titania Nanofibers Synthesized by Sol-Gel and



693 Electrospinning Techniques. *Journal of Engineered Fibers and Fabrics*. **5**(1), pp.50-  
694 56.

695 Sugiyama, K. and Takéuchi, Y. 1991. The crystal structure of rutile as a function of  
696 temperature up to 1600°C. *Zeitschrift für Kristallographie*. 194. p.305. [Accessed  
697 2014-07-02t14:40:58.733+02:00]. Available from:  
698 [http://www.degruyter.com/view/j/zkri.1991.194.issue-3-4/zkri.1991.194.3-  
699 4.305/zkri.1991.194.3-4.305.xml](http://www.degruyter.com/view/j/zkri.1991.194.issue-3-4/zkri.1991.194.3-4.305/zkri.1991.194.3-4.305.xml).

700 Takagi, M. 1954. Electron-Diffraction Study of Liquid-Solid Transition of Thin Metal Films.  
701 *Journal of the Physical Society of Japan*. **9**(3), pp.359-363.

702 Tang, H.Berger, H.Schmid, P.E.Lévy, F. and Burri, G. 1993. Photoluminescence in TiO<sub>2</sub>  
703 anatase single crystals. *Solid State Communications*. **87**(9), pp.847-850.

704 Wronski, C.R.M. 1967. The size dependence of the melting point of small particles of tin.  
705 *British Journal of Applied Physics*. **18**(12), p1731.

706 Xia, Y.Yang, P.Sun, Y.Wu, Y.Mayers, B.Gates, B.Yin, Y.Kim, F. and Yan, H. 2003. One-  
707 Dimensional Nanostructures: Synthesis, Characterization, and Applications.  
708 *Advanced Materials*. **15**(5), pp.353-389.

709 Yang, J.Mei, S. and Ferreira, J.M.F. 2001. Hydrothermal Synthesis of Nanosized Titania  
710 Powders: Influence of Tetraalkyl Ammonium Hydroxides on Particle Characteristics.  
711 *Journal of the American Ceramic Society*. **84**(8), pp.1696-1702.

712 Zhang, H. and Banfield, J.F. 2000. Understanding Polymorphic Phase Transformation  
713 Behavior during Growth of Nanocrystalline Aggregates: Insights from TiO<sub>2</sub>. *The  
714 Journal of Physical Chemistry B*. **104**(15), pp.3481-3487.

715 Zhang, H.Chen, B.Banfield, J.F. and Waychunas, G.A. 2008. Atomic structure of nanometer-  
716 sized amorphous TiO<sub>2</sub>. *Physical Review B*. **78**(21), p214106.

717 Zhang, H. and F. Banfield, J. 1998. Thermodynamic analysis of phase stability of  
718 nanocrystalline titania. *Journal of Materials Chemistry*. **8**(9), pp.2073-2076.

719 Zheng, L.Xu, M. and Xu, T. 2000. TiO<sub>2-x</sub> thin films as oxygen sensor. *Sensors and  
720 Actuators B: Chemical*. **66**(1-3), pp.28-30.

721